LRP 569/97 February 1997

COMPARISON OF THE CREATE-L PLASMA RESPONSE MODEL WITH TCV LIMITED DISCHARGES

F. Villone, P. Vyas, J.B. Lister, R. Albanese

COMPARISON OF THE CREATE-L PLASMA RESPONSE MODEL WITH TCV LIMITED DISCHARGES

F. Villone[1], P. Vyas, J.B. Lister and R. Albanese[2]

Centre de Recherches en Physique des Plasmas
Association EURATOM-Confédération Suisse
CRPP-EPFL, CH-1015 LAUSANNE

[1] Consorzio CREATE, Dipartimento di Ingegneria Industriale
Università di Cassino, Via Di Biasio 43, I-03043 CASSINO

[2] Consorzio CREATE, DIEMA, Università di Reggio Calabria,
Via Cuzzocrea 48, I-89128 REGGIO CALABRIA

ABSTRACT

Experiments have been performed on the TCV tokamak to evaluate the response of Ohmic, L-Mode, limited, vertically unstable plasmas to changes in all the poloidal field coil voltages. The resulting closed loop plasma responses have been compared with the CREATE-L linearised MHD equilibrium model of TCV. All the responses in both the time domain and the frequency domain show excellent agreement both for directly measured quantities and for derived parameters which can be used as feedback variables. No modifications to the CREATE-L model were made to achieve this quality of agreement, indicating that the underlying physical assumptions are appropriate.

1. INTRODUCTION

The shaping and control of present tokamaks is often simple but adequate. The design of the feedback controllers is usually based on primitive modelling of the plasma itself, taking into consideration the plasma inductance and the vertical positional instability inherent in elongated plasmas. The positioning of the poloidal field (PF) control coils is crucial to the design of the controller, but the presence of the vessel is usually only taken into account for the control of the vertical position. Although the present degree of control is adequate, it is likely that improvements could be made by considering a more detailed model of the tokamak. Such controllers can be designed to optimise the performance of the tokamak given a model, using a variety of techniques. To our knowledge, the only strictly model-based controller used on a tokamak has been for the vertical position control of COMPASS-D, in which an experimentally derived model was used to develop controllers avoiding problems which had been encountered in the control loop [1]. The essential component of a model-based controller is of course the model, which must be sufficiently accurate that the feedback loop has the predicted performance.

At present there is a considerable interest in the validity of different proposed models of the response of a tokamak plasma to changes in the surrounding currents, both in the passive tokamak structures and in the PF control coils. This interest is motivated by the challenge of designing a suitable PF coil system and PF control system which meets the requirements of the ITER tokamak and which is not over-designed. Questions of limited power, limited voltage and above all limited cost all push the design of the PF system towards the minimum solution. Many plasma models are currently being used during the ITER design and their physics content and assumptions differ considerably. It was considered essential to commence on a procedure of extensive validation of one of these models on an existing tokamak. We have chosen the CREATE-L model, presented in detail in Section 2, since it is widely used by the European Home Team in the ITER design and since it is relatively simple while remaining based on a physical model of the plasma equilibrium. It is a linearised model, allowing its straightforward use in the design and testing of feedback controllers in simulations.

Previous experimental work has concentrated on the control of the unstable vertical position of elongated plasmas, which has so far presented the greatest challenge. Model comparisons of only the vertical motion have been carried out on C-MOD in open loop and closed loop [2], on DIII-D in closed loop [3], on TCV in both closed loop [4] and open loop [5], on JT-60 Upgrade in closed loop [6], as well as on COMPASS-D in open loop [7].

This present paper presents a further step in this validation process, in which we have concentrated on a particularly simple plasma equilibrium, namely a limited, Ohmic, L-mode, up-down symmetric and vertically centred discharge of modest vertical instability growth rate. As such, this paper is a natural extension to previously reported work on the TCV tokamak in which only the vertical plasma motion was studied with the feedback loop closed and then only compared with a simple rigid current displacement model (RCDM) [4].

The TCV tokamak, of which the poloidal cross section is illustrated in Fig. 1, is an almost ideal device on which to perform this type of study, for several reasons. The tokamak is constructed with no significant quantity of ferromagnetic material, removing one of the greatest obstacles to obtaining good agreement between models of the PF system and experiment. TCV is equipped with a large number of PF coils, providing a large variety of responses to coil current changes, all of which can be compared with the model. The PF coils are all powered by separate supplies, allowing total freedom of changes to the separate coil voltages. The diagnostics are comprehensive, with 38 poloidally distributed measurements of the poloidal field and the poloidal flux, all of which have been calibrated with great care [8].

In the previous work [4], the vertical position response to current changes was explored using two methods of exciting the feedback control loop. Square voltage pulses were applied to individual coil pairs, but always in up-down antisymmetric combinations to impose only radial field variations at the centre of the plasma. These pulses provided time responses of the perturbed quantities which were easily compared with the equivalent time domain responses of the RCDM model. Quantities such as the

low frequency gain, the overshoot and the rise time of the responses were easily judged by eye. Excitation of the same coil combinations using a Random Binary Sequence (RBS) of coil voltage perturbations did not lend itself to a simple visual comparison, but it provided a very rich excitation over a wide range of frequencies, allowing a subsequent comparison of the mean square response.

In the present work, we have retained the approach of studying the response to both square wave excitation and RBS excitation and have compared the responses with the CREATE-L model as well as with the RCDM model, in both time and frequency domains. We have added up-down symmetric coil pair excitation, exciting changes in up-down symmetric quantities such as the plasma current, major radius, elongation and triangularity. The CREATE-L model is used to compare these new excitation combinations in both time and frequency domains. The 10 additional excitation combinations, comprising the Ohmic Heating (OH) coils and the symmetric E and F coil pairs, plus the 8 previous combinations, lead to a total of 18 separate experiments for each of the time and frequency domains. A further extension in this work is a greater degree of attention to the modelling of the power supplies and greater attention to the precise details of the feedback loop electronics, motivated by the quality of the agreement we found. While increasing the variety of the responses of the plasma to the excitations applied, we also examine the response of the individual diagnostic signals as well as the feedback control loop control parameters and some low moments of the current distribution.

When comparing the experimental results with the predictions of the CREATE-L model, we shall come across a new issue, concerning the importance of the plasma model itself to the accuracy of the simulations. The up-down symmetric responses of the raw data signals can be fairly well approximated with a plasmaless model. We will therefore address the question of which observable parameters can be used to examine the plasma part of the model with the greatest discrimination. In order to do this, we construct the same CREATE-L model of the TCV closed loop, but without the plasma. The resulting closed loop model will be referred to as the plasmaless CREATE-L model.

The paper has the following structure. In Section 2 we present the CREATE-L linearised model of the TCV plasma response and the plasma control feedback loop. In Section 3 we investigate a single up-down antisymmetric coil pair excitation and a single up-down symmetric coil pair excitation of the PF coils. These two experiments are presented in detail to develop a methodology and to discuss the different issues. In Section 4 we present the complete study of all combinations of all the possible coil excitations to generalise the conclusions of Section 3. Section 5 is devoted to a discussion of the results and a discussion of the limitations on the conclusions which can be drawn. In Section 6 we present our conclusions.

2. THE CREATE-L MODEL OF TCV PLASMAS

The full CREATE-L model of the linearised response of a TCV plasma can be considered as containing three basic components. The first component describes the general response of a plasma to changes in the currents in the passive structures of the vessel or currents in the active poloidal field coils. This plasma response will depend on the particular plasma equilibrium and of course on the tokamak geometry. The second component essentially quantifies the vacuum properties of the active poloidal field coils and passive structures of the tokamak, including their physical location, their resistances and their mutual inductances. The third component comprises the modelling of the diagnostic signals used as inputs to the TCV control loop and the properties of the feedback controller and includes the power supplies. All of these three elements must be adequately resolved for the full CREATE-L model to simulate a TCV plasma accurately. We discuss the construction of the CREATE-L model in the rest of this section, concluding with a description of the simulation environment.

2.1. The plasma response

The CREATE-L model [9] is a natural evolution of work previously described [10]. The plasma is assumed to be in a permanent MHD equilibrium for all timescales. There is therefore no requirement to take into account the limited acceleration of the plasma due to its finite mass. This reduces the timescale of the evolution of plasma equilibrium

changes to the timescales with which fluxes at the plasma boundary can change following penetration through the conducting structures around the plasma. A second assumption is that the toroidal plasma current density profile $Jp(r,\Psi)$ is assumed to be a function of only three parameters which are associated with specific physical quantities, namely Ip (the total plasma current), l_i (the plasma internal inductance) and β_p (the plasma poloidal beta). This simplification corresponds to the well-known property of the inverse problem, that additional information on current or density profiles is difficult to obtain from magnetic measurements outside the plasma. As a consequence of this, two different plasma equilibria, with different current density or plasma energy profiles, but the same Ip, l_i, and β_p, will have almost the same electromagnetic interaction with the surrounding conductors [11].

Any variations of l_i and β_p are treated non-consistently as external disturbances, however the evolution of the plasma current Ip is determined consistently by Ohm's law:

$$\boldsymbol{E} + \boldsymbol{v} \times \boldsymbol{B} = \eta \boldsymbol{J} \tag{2.1}$$

where $\boldsymbol{E}$ is the electric field, $\boldsymbol{B}$ is the magnetic field, $\boldsymbol{v}$ is the velocity, $\boldsymbol{J}$ is the current density and η is the resistivity tensor.

Equation (2.1) coupled with the requirement of MHD equilibrium yields:

$$\int_{Vp} \boldsymbol{E}_{tor} \cdot \boldsymbol{J}_{tor} \, dV = \int_{Vp} (\boldsymbol{J} \cdot \eta \boldsymbol{J} + \boldsymbol{v} \cdot \nabla p - \boldsymbol{E}_{pol} \cdot \boldsymbol{J}_{pol}) \, dV \tag{2.2}$$

where V_p is the plasma region, p is the pressure, and the subscripts "tor" and "pol" denote toroidal and poloidal components, respectively.

The R.H.S. of (2.1) can be neglected in the limit of highly conductive, low pressure, large aspect ratio plasmas, in which case we can set:

$$\int_{Vp} \boldsymbol{E}_{tor} \cdot \boldsymbol{J}_{tor} \, dV = -\int_{Sp} J_p \, \partial\psi/\partial t \, dS = 0 \tag{2.3}$$

where S_p is the plasma cross-section, J_p is the toroidal component of the plasma current density, ψ is the poloidal magnetic flux and t is the time.

The time evolution of the plasma response is determined by (2.3) and by all the additional circuit equations:

$$d\Psi/dt + \mathbf{R}\, I = V \tag{2.4}$$

where I is the set of currents flowing in the external (active and passive) conductors, Ψ is the set of fluxes linking these currents, $\mathbf{R}$ is the diagonal resistance matrix of the circuits and V is the complete set of applied voltages, with $V=0$ for the passive circuits. This approach is also applicable to both axisymmetric and three-dimensional passive conductors, by approximating the full current distribution with a set of equivalent discrete conductors.

The derivation of the linearised model from equations (2.3)-(2.4) in the absence of any external disturbances is now straightforward:

$$\mathbf{L}^* \, dx/dt + \mathbf{R}\, x = u \tag{2.5}$$

in which the internal state vector is $x = [\delta I, \delta I_p]^T$ and the input vector is $u = [\delta V, 0]^T$. The quantities δI, δI_p and δV represent linearised deviations about their nominal values. The matrix $\mathbf{L}^* = \partial[\Psi, \Psi_p]^T / \partial[I, I_p]^T$ is the modified inductance matrix, which differs from the vacuum inductance matrix as a result of the influence of the plasma. The quantity Ψ_p is the flux linked to the plasma weighted by the unperturbed plasma current I_{po} and the plasma current density J_{po}:

$$\Psi_p = \int_{Sp} J_{po}\, \psi \, dS / I_{po} \tag{2.6}$$

Since this is precisely the part of the model which depends on the particular plasma equilibrium, we use a reconstructed estimate of the equilibrium of the discharge to be simulated, obtained using the LIUQE inverse equilibrium code [12]. Equation (2.5) can be converted to the standard state space representation used widely in control theory:

$$dx/dt = \mathbf{A}\, x + \mathbf{B}\, u \tag{2.7}$$

where the matrix determining the poles of the system is $\mathbf{A} = -\mathbf{L}^{*-1}\mathbf{R}$ and the matrix describing the coupling between the applied voltages and the internal states is $\mathbf{B} = \mathbf{L}^{*-1}$

The linearised model can also predict linearised output parameters y other than the state variables themselves, such as field or flux measurements, separatrix gap deviations or velocities for diverted plasmas [9] using the standard output equation:

$$y = \mathbf{C}\,x + \mathbf{D}\,u \tag{2.8}$$

where **C** and **D** are the state-to-output and input-to-output matrices, respectively.

The presence of possible β_p and l_i disturbances can be taken into account by introducing two additional matrices **E** and **F** such that

$$dx/dt = \mathbf{A}\,x + \mathbf{B}\,u + \mathbf{E}\,dw/dt \tag{2.9}$$

$$y = \mathbf{C}\,x + \mathbf{D}\,u + \mathbf{F}\,w \tag{2.10}$$

where $w = [\delta\beta_p, \delta l_i]^T$. These matrices **E** and **F** are determined using the system response to canonical disturbances [8]. Since w is effectively a disturbance to the system, we must know its behaviour *a priori*; in other words, β_p and l_i drops are not calculated in a self-consistent fashion. The **E** and **F** matrices are not used in this present paper, since we shall only be considering external actions on the plasma, via the coil voltage vector V.

The model expressed in the compact form of equations (2.9) and (2.10) is immediately useable in computer simulations using standard techniques and represents the final form of the CREATE-L open loop model used in this work.

2.2. The TCV electromagnetics

The matrix elements of the various components of the linearised open-loop model equations (2.9-2.10) must be determined for the TCV geometry. This was carried out using a standard finite element technique, using a mesh with 2784 nodes and 1367 second order triangular elements. The passive structure of the vacuum vessel was approximated using a set of 56 axisymmetric conductors carrying a uniform current density, their resistances being chosen to fit the TCV measurements of the vessel resistivity [8], giving a total vessel resistance of 49.1 μΩ. The TCV vessel has a skin diffusion time of the order of 80 μsec and we neglect this. The active coils, Fig. 1, have been similarly described as 23 conductors carrying uniform current densities. Their

interconnections are taken into account, leading to a total of 18 independently powered circuits, 2 for ohmic heating (OH) and 16 for shape control (E and F). Consequently, the number of states **x**, defining the state equation model order is 75 (56 for the vessel currents, 18 for the coil currents and 1 for the plasma), while the number of inputs $\boldsymbol{u}$ is 18, namely the voltages fed to each independent circuit.

The TCV control loop uses the outputs from 38 poloidal magnetic field pick-up coils, 38 magnetic flux loops and the measurements of 18 poloidal field coil currents. In order to simulate the control loop and compare the experimental and simulated data, we need to provide the **C** matrix of Equation (2.10) to output all 94 outputs in the vector $\boldsymbol{y}$. This was performed by taking the known coordinates of the magnetic field pick-up coils, essentially sensitive to the poloidal magnetic field parallel to the vacuum vessel wall and the magnetic flux loops, of which some are toroidally complete and some are toroidally incomplete saddle coils. Figure 1 indicates the location of these measurement points. The active coil currents are directly obtained from the internal state vector.

2.3. The TCV plasma control system and power supplies

The details of the TCV control system, both hardware and software, are described extensively in [13] and we recall only those details relevant to the modelling of the control loop. The TCV plasma control is a Multiple Input Multiple Output (MIMO) closed loop system, consisting of standard PID controllers acting on a set of error signals (Fig. 2). The details of the controlled variables and of the derivation of the controller are as described earlier [4]. The stimulation signals used in these experiments are added directly to the voltage outputs of the controller.

Firstly, we address the question of the parameters under feedback control, only considering the electromagnetic parameters, disregarding of course the density control. The control parameters are constructed in real time using digitally controlled analogue hardware [14], taking linear combinations of the 38 poloidal flux, 38 poloidal field and 18 poloidal field coil current measurements available. These measurements are provided by the **C** matrix as described. This formation of the control parameter values ($\boldsymbol{cp}$) is exactly reproduced in the estimator matrix, Fig. 2, allowing the CREATE-L model to

produce the simulated values of the control parameters using the same weights as in the experiment. At the same time, it was possible to compare the input diagnostic signals and to compare plasma parameters which were not actually used in the control loop. The controlled parameter estimators are optionally scaled provided by the hardware are compared with a reference signal ($\boldsymbol{cp}_{\mathrm{ref}}$) which, for all parameters other than the plasma current itself, is optionally scaled with the plasma current. For the linearised simulations the reference values are zero. Instead the control parameters $\boldsymbol{cp}$ are scaled using matrix $\mathbf{K_2}$ in the feedback loop.

The controller is defined by three matrices whose inputs are the control parameter errors ($\boldsymbol{e}$) and whose outputs are requested rates of change coil current. These outputs are then post multiplied by a mutual inductance matrix $\mathbf{M}$ to provide feedback voltages which are summed with a pre-programmed voltage to provide the power supply demand voltage. Any perturbations are contained in the pre-programmed signals $\boldsymbol{Q}$ in a period of the discharge during which the pre-programming of the reference and voltage signals is constant with time. The three controller matrices provide proportional signal gain, integral signal gain and differential signal gain to create a decoupled generalised PID controller. The algorithm for defining the feedback gains is described in previous work [4].

One option of operating the TCV power supplies is to crudely preprogram the PF coil currents and require each power supply to maintain the individual currents close to their pre-programmed values using a weak purely proportional controller, referred to as the hybrid power supply mode. Feedback control is provided by the voltage demand signal described above and which is summed with the internal current controller signal. Such a method of controlling the power supplies provides an effective additional resistance to the individual coils, since it counteracts any change in a PF coil current with a proportional change in the coil voltage. The sum of the physical coil resistance and this dominant effective additional resistance was calibrated experimentally for each PF coil and subsequently used in the simulations. This feedback loop is shown in Fig. 2 where the diagonal matrix $\mathbf{K_1}$ provides the effective additional resistance. The pre-programming of the reference current waveforms provides additional constraints which

uniquely determine them, given more coil voltage inputs than feedback controlled parameters.

Finally, a power supply (PS) model must be considered. Each PS consists of a 12-phase thyristor AC-DC converter [13], which introduces both a ripple due to the thyristor firing and a delay due to the switching times at which the thyristors are fired. Such a supply is highly nonlinear but was approximated as a linear system. We chose to disregard the ripple, which is mainly filtered by the vessel, and to model the PS using only a single pole filter, approximating the time delay and bandwidth of the PS. The magnitude of the pole was tuned to match the observations, as discussed later.

2.4. The TCV closed loop simulations

The overall linearised closed loop model of TCV can be constructed from the basic elements described, as in Fig. 2. All the elements are linear and time invariant and have finite dimension. Given the values of the matrices modelling the single blocks, it is therefore straightforward to obtain the overall transfer function and to perform a time evolution simulation. A 0.5 second plasma simulation requires about 15 seconds of computation, once the open loop model has been calculated. Creating a new open loop model for a different plasma equilibrium takes up to an hour. In all the work presented, we have assumed that the plasma equilibrium remains fixed during the discharge flat top. Although the experimental data contain drifts, the assumption that the linearisation remains constant is reasonable.

It is important to emphasise that at no time was the basic TCV model or the CREATE-L plasma model "tuned" to enhance the agreement in the results which follow.

3. METHOD OF COMPARISON

Many experiments were performed, providing a large range of plasma responses, to investigate thoroughly the CREATE-L model. This section describes

a) the different stimulation methods defining the inputs chosen, and the choice of input signals,

b) the choice of plasma parameters examined (the output variables),

c) the analysis used for the comparison between model and experiment, and

d) the criteria used to assess the accuracy of the model.

Only some examples of the experimental data will be used to illustrate the issues described in this section. However the full results will be presented in Section 4.

As already mentioned, the RCDM model was tested previously with limited up-down symmetric plasmas using up-down antisymmetric coil pair stimulation. The symmetry of the vessel and plasma allowed the excitation of only the plasma vertical motion which was adequately described by the RCDM model. Square pulses and RBS signals were used to excite the control coils. These stimulation signals are used here to test the responses of the CREATE-L model in both the time (square pulse) and the frequency domains (RBS). The procedures used to derive the results are presented in the first subsection.

In addition to the vertical movement, the CREATE-L model provides shape and position responses to excitation from any coil or combination of coils. Up-down symmetric coil pairs were chosen to excite other plasma parameters, again with square pulses and RBS signals. For these experiments, the symmetry of the TCV vessel and coils was exploited to prevent vertical plasma motion. A small set of parameters was chosen for comparison and the reasons for their selection are discussed below. The time domain and frequency domain analysis methods are the same as for the antisymmetric excitation.

3.1. Antisymmetric excitation

The E and F poloidal field coils (Fig. 1) were grouped into 8 pairs, each coil being the same distance from the midplane and the same side, either inboard or outboard of the TCV vessel. Each pair is stimulated at separate times from other pairs, either with one discharge for each pair in the case of RBS signals, or using different time windows within a single plasma discharge for square pulse stimulation.

The chosen stimulation signal was added to the power supply input signal for one of the coils in a pair and subtracted from the other coil in the pair. The experimental TCV data were then compared against the CREATE-L model and the RCDM model responses. The procedures used to perform the comparison are illustrated by examples in the following sections. Coil pair E4-E5 is used in the examples below because it is found to have the highest bandwidth, as in [4], and therefore has a good signal to noise ratio.

3.1.1. Time domain response using square pulses

Figure 3 shows an example of a pulse with the coil current and zI_p responses for the E4-E5 coil pair. The pulses had amplitudes in the range 70V to 500V and a width of 50ms. The amplitudes were chosen for each coil pair as the minimum required to observe a clear signal above the noise in the response. Too large an amplitude would lead to a more nonlinear response. The amplitudes were also constrained by the power supply voltage ranges, +/-700V for the E coils and +/-1400V for the F coils, and the need to limit the forces acting on the vessel. The signal source generators interpolate linearly between samples at 1ms intervals, i.e. the signal ramps between the two levels during a 1ms interval. The modelled and experimental signals are overlaid as in Fig. 4. A least squares straight line fit was removed from both the experimental data and simulation responses to remove their offsets and linear drift. This is because the low frequency disturbance or drift experienced by the plasma was not modelled in the simulations. An advantage of the pulse responses is that the experimental data can be compared against the simulated responses and simply assessed visually. The pulse causes a step-like closed loop response in the control voltages and currents and also the zI_p signal. The main features that can be observed from the traces are those typical of a low order system, as was observed in DIII-D [3]. These are the overshoot and natural frequency, and the low frequency gain. Integral feedback in the controller ensures that the disturbance is rejected at very low frequencies.

Figure 4 contains three responses for the model, corresponding to different values of the power supply time constant used in the simulations. For the coil pair E4-E5, a small or no time constant produces overdamped responses, whereas too long a time constant

(0.6ms) produces highly oscillatory responses. This sensitivity of the model to the power supply pole indicates that the stability margin is relatively poor. For these experiments the plasma has an instability growth rate of approximately $260s^{-1}$ and the closed loop response is sensitive to the open loop model. The value of the power supply time constant was tuned until the model responses matched the experiment. The best value of 0.3ms is consistent with a previous estimate derived from the fact that they are 12-phase thyristor converters with a supply frequency of approximately 110Hz. The power supply pole was then fixed at 1/0.3ms for all the other simulations, whether symmetric or antisymmetric, square pulse or RBS stimulation. It was noticed that the power supply pole had very little effect on the model responses when stimulated using symmetric excitation.

The results in Section 4 are presented as in Fig. 5. Here the experimental data are plotted against simulations using both the CREATE-L model and the RCDM model. Quantifying the agreement of the models for all cases proved not to be possible. Instead subjective assessments were made based on the shape of the overshoot and factors such as the rise time, degree of damping and frequency. These features were examined visually and used to determine whether the data invalidated the model in any way. Qualification of the agreement was left for the frequency domain.

3.1.2. Frequency domain response using RBS

Square pulse responses provide an easy method of comparing a model with an experiment. However the frequency content of the square pulse input signal is limited and only the dominant modes of the closed loop system can be observed in the response. A more thorough comparison should test the plasma and model over a larger range of frequencies and excite all the modes of the system. Such a signal is termed a persistently exciting signal in system identification theory, which is the general process of fitting mathematical models to experimental data. An RBS signal provides such a persistently exciting stimulation signal and spectral analysis was used to estimate the closed loop frequency response functions. These were compared with the frequency response functions calculated directly from the closed loop model.

The input signal (Fig. 6) switches between two levels at random with probability of 0.5 at time intervals of 1ms. As with the square pulses, the waveform generator interpolates linearly between 1ms samples. The amplitude of the stimulation applied was +/-100V for both the E coils and the F coils. The short switching interval introduces high frequency components into the signal allowing a broad range of frequencies to be examined. Switching between two levels maximises the variance of the signal whilst limiting the peak amplitude. Hence the signal to noise of the zI_p output signal is adequate given modest power supply stimulation.

The RBS experiments previously presented [4] were used for the CREATE-L comparison. The plasma equilibrium in these experiments was slightly different than for the square pulse experiments. The vertical position instability growth rate was lower at $160s^{-1}$. A different CREATE-L model was derived with appropriate l_i and β_p values for these simulationsThe resulting responses of the coil currents and of zI_p are also shown in Fig. 6 for the E4-E5 coil pair. Eight plasma discharges were required to test each of the E and F coil pairs, with the stimulation applied for at least 500ms during the discharge flat top.

The time domain comparisons for the square pulse experiments can be made simply by overplotting experiment and model data. However the process of analysing the RBS experiments is more involved because a suitable method must be chosen to obtain the frequency response function of the system from the input and output data. The method must also provide clear results in the presence of poor signal to noise levels and if possible provide an indication of the accuracy of the estimates.

The simplest approach is to take the Discrete Fourier Transform (DFT) of the output signal and divide by the DFT of the input signal. Such an estimate is termed the Empirical Transfer-function Estimate (ETFE) in [15]. For the E4-E5 coil pair the amplitude spectra of the stimulation and the zI_p signals are shown in Fig. 7. When dividing one by the other the result is a noisy curve also shown in Fig. 7.

For an RBS input signal, the variance of the estimate depends on the signal to noise ratio of the system. It is not a consistent estimate in that the variance does not decrease

if the length of time for which the stimulation is applied is increased. This can be understood when considering that the DFT of 512 samples of data would provide estimates at 256 frequencies. Using twice as many samples would not reduce the variance but instead produce estimates at twice as many frequencies. It can often be assumed that the transfer function of a system is a smooth function of frequency and since the estimates at different frequencies are asymptotically uncorrelated, it is possible to average estimates at neighbouring frequencies to reduce the variance. Spectral analysis is a different system identification method which can be interpreted as being a smoothed version of the ETFE [15]. This technique was used to produce the smoother curve in Fig. 7 along with the confidence bounds and is a commonly used method [16]. We summarise this method in detail to derive the confidence bounds which we will use as part of the comparison.

A linear system can be characterised by its impulse response $g(t)$ or its frequency response function $G(\mathrm{j}\omega)$. In the time domain, the output of the system $y(t)$ is related to the input $u(t)$ by the convolution integral

$$y(t) = \int_0^\infty g(\tau)u(t-\tau)\,\mathrm{d}\tau\,. \tag{3.1}$$

Taking the Fourier Transform gives $Y(\omega)=G(\mathrm{j}\omega)U(\omega)$. A similar relationship exists $S_{uy}(\omega)=G(\mathrm{j}\omega)S_{uu}(\omega)$, where S_{uu} is the autospectral density function and S_{uy} is the cross-spectral density function. The frequency response function can be derived simply by dividing S_{uy} by S_{uu}.

To estimate the frequency response function it is first necessary to estimate the spectral density functions from the data. Given signals $u(t)$ and $y(t)$ of unlimited length T, S_{uu} and S_{uy} can be defined as

$$S_{uu}(\omega) = 2\lim_{T\to\infty}\frac{1}{T}\mathrm{E}\left[\left|U(\omega,T)\right|^2\right] \tag{3.2}$$

and

$$S_{uy}(\omega) = 2\lim_{T\to\infty}\frac{1}{T}\mathrm{E}\left[U(\omega,T)Y^*(\omega,T)\right] \tag{3.3}$$

where E is the expectation operator and asterisk denotes the complex conjugate. A simple method of estimating S_{uu} would be to square the amplitude response from the

Fourier transform of a given record of data $u(t)$ taken over a length of time T. However, as in the case of the ETFE, this estimate would be inconsistent since the variance of the estimate would again be independent of the length of data T. In practice the variance of the estimates are reduced by segmenting the data into n_d separate sections each of length T_d, calculating the Fourier transform for each section and then using the average to form a "smooth" estimate

$$\hat{S}_{uu}(\omega) = \frac{2}{n_d T_d} \sum_{i=1}^{n_d} \left| U_i(\omega, T_d) \right|^2 \tag{3.4}$$

The normalised rms error for the estimate of S_{uu} is

$$\varepsilon\left[\hat{S}_{uu}(\omega)\right] = \frac{\sigma\left[\hat{S}_{uu}(\omega)\right]}{S_{uu}(\omega)} = \frac{1}{\sqrt{n_d}} \tag{3.5}$$

A similar procedure can be used to estimate S_{uy}. In practice, when calculating these estimates, Hanning windows are used to reduce the effect of spectral leakage. This tapers the signal at the beginning and end of each time window to zero, reducing the information in each segment and therefore increasing the variance of the estimates. Some of the information can be recovered by overlapping the segments. For the estimates in this paper the segments were overlapped by 50% which is a commonly used choice of overlap and recovers 90% of the information lost due to the tapering [16].

The coherence function $\gamma_{uy}^2(\omega)$ is a measure of the portion of the output signal $y(t)$ at frequency ω which is due to the input $u(t)$.

$$\gamma_{uy}^2(\omega) = \frac{\left| S_{uy}(\omega) \right|^2}{S_{uu}(\omega) S_{yy}(\omega)} \tag{3.6}$$

It is used in the calculation of the confidence bounds of the frequency response estimates. When $\gamma_{uy}^2(\omega)$ is zero then the input and output are unrelated. The case of $\gamma_{uy}^2(\omega) = 1$ corresponds to the ideal case when $y(t)$ is related to $u(t)$ via a linear system with no extraneous noise. The spectral density estimates with their normalised errors can be used to estimate the frequency response function and provide confidence bounds for the amplitude response function $|\hat{G}|$

$$\mathrm{Var}\left[\left|\hat{G}\right|\right] \approx \frac{\left(1-\gamma_{uy}^2\right)\left|G_{uy}\right|^2}{2\gamma_{uy}^2 n_d} \tag{3.7}$$

and for the phase response function $\hat{\phi}_{uy}$

$$\mathrm{Var}\left[\hat{\phi}_{uy}\right] \approx \frac{\left(1-\gamma_{uy}^2\right)}{2\gamma_{uy}^2 n_d} \tag{3.8}$$

These equations are valid when the segments used to estimate the spectral density functions are not overlapping, so here they are used as guides rather than in a strict statistical sense. Having established the method the results for coil pairs E4-E5 are presented in Fig. 8. Both the amplitude and the phase spectra are plotted and compared against the RCDM and CREATE-L models. The confidence bounds represent 3 standard deviations of the frequency response estimate.

When assessing the agreement of the models, the first concern should be that the model responses lie within the confidence bands for all frequencies. This is easily judged with a plot such as Fig. 8. A more quantitative assessment of the model is to measure how small the model error is relative to the size of the confidence bounds. A set of 100 logarithmically spaced frequency points ω_i between 10 and 300Hz was chosen to make the comparison. Below 10Hz the frequency response function is not easily identifiable because of the short duration of the time segments used to estimate the spectral densities. Above 300Hz the noise component in the signals become significant making the estimate itself noisy. The error E_{MC} between the amplitude spectrum of the CREATE-L model $M_{\mathrm{C}}(\omega)$ in dB and the experimental value $M_{\mathrm{E}}(\omega)$ also in dB can be calculated from

$$E_{\mathrm{MC}}^2 = \frac{1}{100}\sum_{i=1}^{100}\left(M_{\mathrm{C}}(\omega_i) - M_{\mathrm{E}}(\omega_i)\right)^2 \tag{3.9}$$

The error E_{MR} between the RCDM model and the experiment can also be calculated by analogy. A measure of the average value of the confidence bounds can be calculated given the 3 standard deviation upper (M_{U}) and lower limits (M_{L}) of the experimental estimates in dB

$$E_{\mathrm{ME}}^2 = \frac{1}{100}\sum_{i=1}^{100}\left(\frac{M_{\mathrm{U}}(\omega_i) - M_{\mathrm{L}}(\omega_i)}{2}\right)^2 \tag{3.10}$$

If the ratio $R_{MC}=E_{MC}/E_{ME}$ is significantly greater than unity then the 'average' model error is significantly greater than the 'average' confidence bound. A simple test of the model would be to verify that this ratio is not significantly greater than unity for all coil pairs. For the E4-E5 coil pair $E_{MC}=1.6$, $E_{ME}=1.4$ and the ratio is $R_{MC}=1.1$, indicating that the model-experiment difference is of the same size as the confidence bound on the amplitude response function estimate. Similar ratios are derived for the phase error in degrees.

3.2. Symmetric excitation

In addition to the vertical position, the CREATE-L model can simulate responses to symmetric stimulations provided by up-down symmetric combinations of PF coils, including the E and F coil pairs as well as the OH1 and OH2 coils. These stimulations change the plasma current, the shape of the plasma and the radial position but do not measurably affect zI_p which we ignore. The plasma was excited with the same two types of stimulation signals as for antisymmetric stimulation, namely square pulse and RBS, and the time domain and frequency domain results are analysed and presented in exactly the same way. The experimental responses are compared with the full CREATE-L model and also the plasmaless model described in Section 2.

The plasma current profile and plasma shape parameters on TCV are reconstructed from measurements of the poloidal field, poloidal flux and its time derivative and the poloidal field coil currents, using the LIQUE inverse equilibrium code [12]. In principle, agreement between the experiment and the model for all of the measured fields, fluxes, voltages and currents would imply the inevitable agreement of all of the deduced plasma shape parameters. We therefore first examine some raw diagnostic information. Figure 9 shows the experimental and modelled responses of two poloidal flux loops to symmetric pulse stimulation of the E4+E5 coil pair. For the flux loop close to the stimulation coils and relatively far from the plasma (loop #7, see Fig. 1), the responses from the CREATE-L model and the plasmaless CREATE-L model are very similar and the agreement with the experimental data is good for both. This is reasonable since the plasma is far away from the loop and has little direct influence. For a flux loop closer to the plasma than to the excitation coils (loop #25) the full CREATE-L and plasmaless

CREATE-L models differ significantly. The full model again agrees well with the experimental results, although the agreement is better for loop #7 than for loop #25.

From these examples, some diagnostic signals are relatively insensitive to the differences between the plasma and plasmaless model for a given stimulation signal and the full model agreement with the experiment is better for some coils than others. When we derive shape parameters, we are implicitly taking sums and differences of the individual signals, for example the radial flux imbalance is the difference between two flux signals and is used to control the radial position of the outermost flux surfaces. The modelling of individual signals may be in good agreement but combinations of them may show significant disagreement.

The control parameters were checked as a first test of the functioning of the closed loop model. For the controller used in the experiments these are: radial flux imbalance (P_VERT), inboard flux curvature (TRI_IN), outboard flux curvature (TRI_OUT), and plasma current (I_p). Figure 10 shows the frequency response of P_VERT to E4+E5 excitation, illustrating the insensitivity of this particular control parameter to the plasma model. This exposes an underlying simplicity in the problem of plasma shape control, since the plasmaless model can perform relatively well for some control parameters, explaining the success of presently used control algorithms relying on this assumption. This implies, however, that the control parameters are not a sensitive enough test to verify the plasma model since they are relatively insensitive to the presence of plasma in the CREATE-L model.

As a next step, we selected parameters approximating the plasma current moments which must be more sensitive to the plasma model, since their response is zero in the plasmaless model. As well as I_p and zI_p, we added a new comparison variable, ψ_R, which is the difference between the R^2I_p current moment and $R_0{}^2I_p$ where R_0 is the unperturbed major radius. The final set of variables tested therefore consists of P_VERT, TRI_IN, TRI_OUT, I_p and ψ_R. These results are presented in full in Section 4 for all the different excitation combinations.

3.3. Summary

The square pulse and RBS stimulation signals provide a variety of means to compare the TCV plasma with different models. When antisymmetric stimulation is applied, only the plasma vertical position is excited and the experimental data are compared with both the CREATE-L model and the RCDM model. When symmetric stimulation is applied, other plasma parameters are excited and the experimental data are compared with two CREATE-L models: one with plasma and one without. The choice of parameters for comparison should ensure that the model is adequately tested for its suitability for control system design and also to test the underlying physics assumptions of the model itself.

4. RESPONSES OF ALL DIFFERENT COIL COMBINATIONS

The results from all the antisymmetric and symmetric square pulse experiments are presented. Four figures directly illustrate the key features of the model responses and whether they are in agreement with the experiments.

The RBS results in the frequency domain provide much more detailed information and would require one figure for each coil and output parameter combination. Instead of presenting all such combinations, the best coil and worst coil model-experiment comparisons are shown for each output parameter. All of the coil and parameter combinations were examined and tables summarising the model-experiment agreement and the confidence bound sizes are presented.

The antisymmetric stimulation results exciting only zI_p are presented first followed by a discussion of the model agreement. The difference in the responses to the different coils pairs is clearly observed and discussed. This is followed by a similar section for the symmetric stimulation experiments.

4.1. Antisymmetric stimulation

The square pulse response to antisymmetric stimulation is shown in Fig. 11 for both E coil pairs and F coil pairs. The experimental traces are overlaid with simulated responses using the CREATE-L model and the RCDM model. The different pairs produce widely varying responses as seen earlier in [4]. For example, E4-E5 produces underdamped responses with a large overshoot whereas F1-F8 produces a damped response with much smaller amplitude. The CREATE-L and RCDM models have very similar responses and both models closely follow the experimental traces. The error between model and experiment is always less than the noise level in the signal. The noise is present in the signal before any stimulation is applied and has an amplitude of +/-250Am. The noise has frequency components up to approximately 200Hz. The main features that can be observed directly from the signals are the overshoot, oscillation frequency, low frequency gain and rise time. These are all in accordance and there is no evidence of any disagreement between the models and the experiment.

The closed loop frequency response functions for a different plasma equilibrium with a lower vertical instability growth rate are shown in Fig. 12. The frequency response functions for the CREATE-L and RCDM models are plotted along with the estimates from experimental data with confidence bounds. The amplitude and phase responses for two different coils are shown, corresponding to the worst and best experiment-model agreement. Differences in fine detail between the RCDM model and CREATE-L model emerge which were not immediately apparent in the time domain responses already examined. These differences persist when modelling the discharge used for the square pulse experiments. Both models follow close to the experiment responses. Both are equally good and it is not possible to rank one model as closer than the other. The deviation between the experiment and models is larger for coil pair F1-F8 than for E4-E5 although it should be noted that the confidence bounds of the frequency response function estimates are much larger and the model traces always lie within the bounds. The size of the confidence bounds is related to the signal to noise ratio of the given frequency component, since when the gain is low the signal to noise is poor and the confidence bounds for coil pair F1-F8 are wider.

Table I includes measures of the average value of the model-experiment error and the average 3 standard deviation confidence bound. The first three rows represent the

average CREATE-L model amplitude error (E_{MC}), the average RCDM model error (E_{MR}) and the average confidence bound value (E_{ME}). The ratios of model error to confidence bound are then listed as R_{MC} for the CREATE-L model and R_{MR} for the RCDM model. For the coil pairs not shown in Fig. 12, when the confidence bounds are close together the model-experiment agreement is very good. When the bounds are large the error can be significant but always within the bounds. For example the confidence bound average for the amplitude of coil pair E3-E6 is 1.3 compared to 3.6 for F2-F7, and the corresponding CREATE-L model-experiment errors are 1.7 and 2.7 respectively. The average model-experiment error for both the CREATE-L and RCDM model is usually of the same order or less than the confidence bound. This is also true for the equivalent phase plots also presented in the table. The subscript "P" replaces "M" to indicate phase rather than magnitude.

The frequency response functions confirm the conclusions in [4] that the coil pair E4-E5 is quicker to act than other pairs. They have a higher bandwidth and higher gain at high frequency (especially around 200Hz) than the F1-F8 pair or indeed any other pair. The phase lag is also smaller in accordance with faster penetration times of the radial field. The stimulation produces a disturbance on zI_p much more quickly than other coils and is very poorly rejected by the loop as can be seen in the step responses.

In conclusion, the antisymmetric excitation experiments do not show any evidence to suggest disagreement between the experiment and either of the CREATE-L or RCDM models.

4.2. Symmetric excitation

The stimulations with symmetric coil pairs excite many more plasma parameters. The plots in Figs. 13 to 15 show the responses of 5 parameters to E, F and OH coil square pulse stimulation. The RCDM model is not able to provide shape responses but alongside the CREATE-L model responses are plotted the responses from the plasmaless CREATE-L model. Some of the control parameters are relatively insensitive to the presence of plasma in the model, as seen for example in Fig. 13 for the TRI_IN control parameter. The plasmaless model response for the current moments are of course

zero and deviations are due to imperfections in the parameter estimator matrix used in the experiments to construct the control parameters. The OH coils provide the largest range of radial position movement (+/-3mm) and these are part of the radial position current moment based Ψ_R responses.

The CREATE-L model agrees well with the experiment responses, especially when the signal to noise ratio is good. A few errors are observed, in the time domain for example in the plasma current response to E2+E7 in Fig. 13. However the deviation is always less than the noise in the signal before any stimulations are applied.

Frequency response functions for the best and worst case model fits are plotted in Figs. 16 to 20. For the three flux-based control variables (P_VERT, TRI_IN and TRI_OUT) the diagrams are relatively clear. The variation in frequency responses is shown by the two different coil pairs and generally when the confidence bound is small the model fit is good. Deviations are noticeable only when the confidence bounds regions are wide. The signal to noise level of the current moment signals are relatively poor generating wide confidence bounds. There is little to suggest that the model is invalidated by the experiment. Tables II to VI confirm that the CREATE-L model-experiment error (E_{MC}) is never much larger than the size of the confidence bound (E_{ME}). This is true also for the plasmaless model (E_{MN}) when compared to the three control parameters (Tables II to IV), but the errors are excessively large when comparing against current moments (Tables V and VI). The same is true for the phase response functions.

4.3. Summary

The overall agreement between the CREATE-L model and the experimental data is good. There is no evidence to suggest that the model is invalidated by the data.

5. DISCUSSION

During initial experiments and simulations, we found some significant divergences between the closed loop model and the experiment. In all cases, these were found to be

experimental problems, due, for example, to saturation of analogue circuitry in the controller integrators or zero crossing problems if a power supply had to change quadrant. Simulating these effects in the model recovered good agreement.

In all of the experiments presented, carried out in well controlled experimental conditions, the agreement between the TCV experimental results and the closed loop simulations using the CREATE-L model is clearly both qualitatively and quantitatively excellent. This implies that the measurements and the model of the control loop are adequate for this level of comparison and that those properties of the CREATE-L model which have an influence on the closed loop behaviour are equally adequate. Certain of the measurements are relatively insensitive to the plasma model and others are totally defined by the plasma part of the CREATE-L model. Extracting the latter properties has allowed us to verify the correctness of the plasma model, by effectively subtracting the vacuum response to the excitations explored. However, the relative insensitivity of some parameters to the plasma model is what makes the derivation of a feedback controller possible without an accurate plasma response model. The controller used in these discharges was based on a simplistic plasma model including the vertical motion, essential to provide a stable closed loop, and a current filament with "typical" inductance.

In order to perform an exhaustive study on all the PF coils, we have had to restrict ourselves to a particular equilibrium, chosen to separate the vertical and radial flux change responses by the symmetry of the plasma itself. This restriction means that several issues remain unexplored by these experiments. These issues must be pointed out and will be addressed in future work on TCV.

The CREATE-L model cannot, by its construction, consider changes to the current profile, except as external l_i changes. The experimental results do not contain a systematic error which suggests that this is necessary, but Ohmic L-mode discharges may not show the problems of current pedestals of additionally heated H-mode plasmas. This should be tested and the experiments with ECRH-heated H-Mode plasmas planned for TCV will provide an ideal opportunity for this.

We have only investigated up-down symmetric plasmas in this paper, but this point will be covered in a systematic study of the response of diverted plasmas with a single X-point (SND) which has started on TCV. We shall investigate such SND plasmas for two reasons. Firstly, there might be differences in the inherent plasma response, for example due to differences in the profiles or due to currents circulating at the X-point. Secondly, we wish to address the question of the geometric response of the separatrix contour which determines the interaction between the plasma and the first wall and the divertor region. A very preliminary evaluation of up-down asymmetric SND plasmas has not shown any important disagreement with the CREATE-L model.

The validation of a plasma model is an important exercise per se, but it also has a practical purpose in that it lays the ground for model based controller design. The question of whether the CREATE-L model as verified is adequate for optimising a high-order controller is an important one. Inclusion of a detailed plasma model into the design of the feedback control law should allow us to develop more precise control algorithms, but these may have the disadvantage of being "tuned" only for a particular discharge. The precision of the comparisons presented in the present paper suggests that considerable improvements might be expected using such a model based controller for the discharge studied. These questions will be explored in subsequent experiments on TCV.

Finally, this work has concentrated on the agreement between the experimental and modelled closed loop response of the plasma control system. Verifying the open loop CREATE-L model of the TCV plasma is a separate issue which is currently receiving attention in TCV experiments.

6. CONCLUSIONS

The work carried out in this paper has shown that the closed loop control of limited, L-Mode, Ohmically heated plasmas in TCV is very well modelled by the CREATE-L linearised plasma response model. During this work, we have made no modifications to this model, confirming its a priori predictive capabilities and allowing its validity to be

generalised to other devices. The response has been explored in the time domain which gives an excellent visual appreciation for the quality of the agreement. The response in the frequency domain is closer to the questions of the design of the feedback control loop and the absence of unexplained features is encouraging for the design of a model based controller for TCV. The restriction to a single plasma equilibrium was essential for this in-depth comparison, but will be lifted in future work.

ACKNOWLEDGEMENTS

It is a pleasure to acknowledge Prof. Guglielmo Rubinacci and Prof. Giuseppe Ambrosino of the CREATE team for stimulating discussions and also the technical support of the TCV team. The quality of the agreement between the modelling and the experimental results would not be achievable without the care and attention to the magnetic diagnostic calibration for which we acknowledge the contributions of Jean-Marc Moret and Felix Buhlmann. Encouragement by the Naka ITER JCT is welcomed. This work was partly supported by a EURATOM mobility contract (FV) and partly by the Fonds national suisse de la recherche scientifique.

REFERENCES

[1] GOSSNER,J.R., VYAS,P., KOUVARITAKIS,B., "Application of Cautious Stable Predictive Control to vertical positioning in COMPASS-D tokamak," University of Oxford Technical Report OUEL 2092/96 (1996), submitted to IEEE Trans. On Control Systems Technology

[2] TINIOS,G., HORNE,S.F., HUTCHINSON,I.H., WOLFE,S.M., Fusion Technology **30** (1996) 201.

[3] LISTER,J.B., et al., Nuclear Fusion **30** (1990) 821.

[4] LISTER,J.B., MARTIN,Y., MORET,J-M., Nuclear Fusion **36** (1996) 1547-1560.

[5] HOFMANN,F., et al., "Vertical instability in TCV: Comparison of experimental and theoretical growth rates," Lausanne Report LRP 562/96 (1996).

[6] HUMPHREYS,D.A., YOSHINO,R., "JT-60 Upgrade Vertical Stability Experiments and Analysis," Japan Atomic Energy Research Institute, Report JAERI-M 92-069 (1992)

[7] VYAS,P., "Plasma Vertical Position Control in the COMPASS-D Tokamak," D.Phil thesis, University of Oxford (1996)

[8] MORET,J-M., BUHLMANN,F., FASEL,D., HOFMANN,F., TONETTI,G., "Magnetic Measurements on the TCV Tokamak," Lausanne Report LRP 521/95 (1996).

[9] ALBANESE,R., et al., "Modelling and engineering aspects of the plasma shape control in ITER," Proc. 19th Symp. on Fusion Technology, Lisbon (Portugal) 1996 (1996); ALBANESE,R., et al., "Plasma current,shape and position control in ITER," Fusion Technology **30** (1996) 167.

[10] ALBANESE,R., COCCORESE,V., RUBINACCI,G., Nuclear Fusion **29** (1989) 1013-1023.

[11] LUXON,J.L., BROWN,B.B., Nuclear Fusion **22** (1982) 813-821.

[12] HOFMANN,F., TONETTI,G., Nuclear Fusion **28** (1988) 1871.

[13] LISTER,J.B., et al., "The Control of TCV Plasmas," Lausanne Report LRP 518/95 (1996), accepted for publication in Fusion Technology.

[14] ISOZ,P.F., LISTER,J.B., MARMILLOD,PH., Proc. 16th Symp. on Fusion Technology, Oxford, 1990 (1991) 1264.

[15] LJUNG,L., "System Identification," Prentice-Hall, Englewood Cliffs, NJ (1987).

[16] BENDAT,J.S., PIERSOL,A.G., "Random Data: Analysis and Measurement Procedures," Wiley, New York (1986)

TABLES

Table I. Antisymmetric RBS excitation, zI_p response error

zI_p	E1-E8	E2-E7	E3-E6	E4-E5	F1-F8	F2-F7	F3-F6	F4-F5
E_{MC}	1.8	2.3	1.7	1.6	4.0	2.7	2.9	2.2
E_{MR}	2.5	2.6	1.5	1.1	4.8	2.1	0.8	1.9
E_{ME}	4.4	1.7	1.3	1.4	7.5	3.6	1.8	3.5
R_{MC}	0.4	1.3	1.3	1.1	0.5	0.7	1.6	0.6
R_{MR}	0.6	1.5	1.1	0.8	0.6	0.6	0.5	0.5
E_{PC}	13.0	13.3	8.4	10.6	29.8	16.8	9.9	8.3
E_{PR}	16.2	18.6	10.9	11.7	29.8	16.0	6.1	11.8
E_{PE}	34.5	11.1	8.8	9.4	117.7	42.2	11.6	18.3
R_{PC}	0.4	1.2	0.9	1.1	0.3	0.4	0.9	0.5
R_{PR}	0.5	1.7	1.2	1.2	0.3	0.4	0.5	0.6

Table II. Symmetric RBS excitation, P_VERT response error

P_VERT	E1+E8	E2+E7	E3+E6	E4+E5	F1+F8	F2+F7	F3+F6	F4+F5	OH1	OH2
E_{MC}	5.3	5.7	7.8	2.0	8.7	8.8	4.1	1.8	2.3	9.2
E_{MN}	7.4	7.1	4.0	3.7	9.7	11.1	6.4	3.9	4.4	10.9
E_{ME}	6.3	5.1	6.5	1.5	5.1	5.3	2.3	2.1	4.0	5.6
R_{MC}	0.8	1.1	1.2	1.4	1.7	1.7	1.8	0.9	0.6	1.6
R_{MN}	1.2	1.4	0.6	2.5	1.9	2.1	2.8	1.9	1.1	2.0
E_{PC}	16.2	32.2	37.5	8.9	44.9	25.3	14.8	13.2	11.5	39.4
E_{PN}	28.6	32.1	34.4	20.6	44.3	24.1	16.7	19.0	25.2	42.4
E_{PE}	49.7	29.8	67.4	9.5	83.1	42.3	14.0	11.9	26.3	92.4
R_{PC}	0.3	1.1	0.6	0.9	0.5	0.6	1.1	1.1	0.4	0.4
R_{PN}	0.6	1.1	0.5	2.2	0.5	0.6	1.2	1.6	1.0	0.5

Table III. Symmetric RBS excitation, TRI_OUT response error

TRI_OUT	E1+E8	E2+E7	E3+E6	E4+E5	F1+F8	F2+F7	F3+F6	F4+F5	OH1	OH2
E_{MC}	5.8	7.4	6.3	3.3	0.8	1.6	2.6	1.6	5.6	2.6
E_{MN}	6.2	7.5	6.2	6.0	0.9	1.5	3.1	2.2	10.3	2.7
E_{ME}	8.5	9.5	10.3	8.2	1.2	1.0	2.7	2.0	5.4	3.5
R_{MC}	0.7	0.8	0.6	0.4	0.7	1.6	0.9	0.8	1.0	0.7
R_{MN}	0.7	0.8	0.6	0.7	0.7	1.5	1.2	1.1	1.9	0.8
E_{PC}	71.9	32.8	68.0	24.5	14.6	5.4	14.0	12.9	38.6	19.1
E_{PN}	76.5	103.3	105.5	141.6	15.4	5.6	12.8	16.1	104.8	19.4
E_{PE}	161.7	80.5	80.6	47.4	7.7	6.6	16.6	12.0	65.2	24.8
R_{PC}	0.4	0.4	0.8	0.5	1.9	0.8	0.8	1.1	0.6	0.8
R_{PN}	0.5	1.3	1.3	3.0	2.0	0.9	0.8	1.3	1.6	0.8

Table IV. Symmetric RBS excitation, TRI_IN response error

TRI_IN	E1+E8	E2+E7	E3+E6	E4+E5	F1+F8	F2+F7	F3+F6	F4+F5	OH1	OH2
E_{MC}	1.3	0.7	8.8	1.3	10.3	9.2	6.5	4.5	8.4	7.3
E_{MN}	1.5	1.2	8.4	1.9	15.9	16.9	12.9	10.6	9.0	8.3
E_{ME}	3.5	0.9	5.9	1.0	6.4	6.5	4.6	3.8	9.9	4.0
R_{MC}	0.4	0.8	1.5	1.4	1.6	1.4	1.4	1.2	0.8	1.8
R_{MN}	0.4	1.4	1.4	1.9	2.5	2.6	2.8	2.7	0.9	2.1
E_{PC}	10.8	7.9	44.6	7.1	44.2	45.6	35.9	28.5	64.6	57.8
E_{PN}	14.5	6.0	46.9	8.1	78.8	72.7	129.6	152.4	64.4	66.8
E_{PE}	18.5	5.9	35.8	6.4	86.9	77.4	65.9	80.6	102.5	258.5
R_{PC}	0.6	1.3	1.2	1.1	0.5	0.6	0.5	0.4	0.6	0.2
R_{PN}	0.8	1.0	1.3	1.3	0.9	0.9	2.0	1.9	0.6	0.3

Table V. Symmetric RBS excitation, I_p response error

I_p	E1+E8	E2+E7	E3+E6	E4+E5	F1+F8	F2+F7	F3+F6	F4+F5	OH1	OH2
E_{MC}	4.0	9.6	8.8	2.6	10.9	9.9	8.7	5.8	4.5	8.3
E_{MN}	17.9	31.5	25.1	29.8	12.5	10.5	22.1	33.4	31.0	13.3
E_{ME}	6.8	3.6	3.9	2.6	6.0	8.6	7.5	6.2	4.6	6.5
R_{MC}	0.6	2.7	2.2	1.0	1.8	1.2	1.2	0.9	1.0	1.3
R_{MN}	2.6	8.9	6.4	11.4	2.1	1.2	3.0	5.4	6.7	2.0
E_{PC}	46.9	10.2	86.1	13.9	63.4	32.2	35.1	26.3	25.6	58.8
E_{PN}	49.9	56.7	77.2	79.8	76.8	35.8	77.1	72.7	63.7	62.6
E_{PE}	86.6	28.7	23.5	16.1	137.3	131.7	52.9	68.0	30.8	98.4
R_{PC}	0.5	0.4	3.7	0.9	0.5	0.2	0.7	0.4	0.8	0.6
R_{PN}	0.6	2.0	3.3	5.0	0.6	0.3	1.5	1.1	2.1	0.6

Table VI. Symmetric RBS excitation, Ψ_R response error

Ψ_R	E1+E8	E2+E7	E3+E6	E4+E5	F1+F8	F2+F7	F3+F6	F4+F5	OH1	OH2
E_{MC}	6.8	3.2	5.1	3.6	4.5	5.0	4.9	1.9	3.5	7.3
E_{MN}	15.8	11.8	16.0	18.1	9.5	10.8	16.3	18.0	11.2	9.8
E_{ME}	6.3	6.1	4.2	7.0	4.5	6.0	4.7	3.9	4.1	4.6
R_{MC}	1.1	0.5	1.2	0.5	1.0	0.8	1.0	0.5	0.8	1.6
R_{MN}	2.5	1.9	3.8	2.6	2.1	1.8	3.5	4.6	2.7	2.2
E_{PC}	40.2	53.5	40.6	18.1	41.0	24.4	20.7	11.4	28.0	52.7
E_{PN}	22.7	29.3	126.5	76.8	74.5	42.9	55.9	50.5	78.0	74.0
E_{PE}	101.8	55.0	90.3	33.0	137.7	36.4	26.2	25.4	69.9	83.3
R_{PC}	0.4	1.0	0.4	0.5	0.3	0.7	0.8	0.4	0.4	0.6
R_{PN}	0.2	0.5	1.4	2.3	0.5	1.2	2.1	2.0	1.1	0.9

FIGURES

FIG. 1. The TCV vacuum vessel, poloidal field coils, poloidal field probes (marked '-' inside the tiles) and flux loops (marked 'x'). The last closed flux surface contours shown (#10857) correspond to limits of variation during up-down symmetric excitation of the E-coils: B_ϕ=1.4T, I_p≈200kA, q_a≈5.

FIG. 2. Schematic diagram of the TCV control system.

FIG. 3. Effect of square pulse stimulation applied to the E4-E5 coil pair.

FIG. 4. Comparison of the experimental response to simulated responses using CREATE-L models with different power supply poles. Square pulse stimulation was applied to coil pair E4-E5. Experimental response (dark solid), model with no power supply pole (dashed), model with pole at 1/0.3ms (light solid), and model with pole at 1/0.6ms (dash dotted).

FIG. 5. Comparison of the experimental response to CREATE-L and RCDM models for square pulse stimulation applied to the E4-E5 coil pair. Experimental response (dark solid), CREATE-L model (light solid), and RCDM model (dashed).

FIG. 6. Effect of RBS stimulation applied to the E4-E5 coil pair.

FIG. 7. a) Discrete Fourier Transform of RBS stimulation signal on the E4-E5 coil pair (dark) and zIp response (light). b) Estimates of closed loop transfer function using ETFE method and spectral analysis. ETFE estimate (light solid), and spectral analysis estimate (dark solid) with associated +/- 3 standard deviation bounds (dotted)

FIG. 8. Bode plot comparison of experimental against CREATE-L and RCDM closed loop transfer function from stimulation on the E4-E5 coil pair to zIp. Experimental spectral analysis estimate (light solid) with associated +/- 3 standard deviation bounds (dotted), CREATE-L model (dark solid) and RCDM model (dotted).

FIG. 9. Comparison of experimental and modelled responses of flux as measured by two different flux loops to square pulse stimulation on the E4+E5 coil pair. Experimental measurement (light solid), CREATE-L model (dark solid) and plasmaless CREATE-L model (dotted).

FIG. 10. Comparison of frequency response functions for the P_VERT control parameter for stimulations using the coil pair E4+E5. CREATE-L model (solid) and plasmaless CREATE-L model (dotted).

FIG. 11. Comparison of the experimental, CREATE-L and RCDM responses to antisymmetric square pulse stimulation on the E and F coils. Experimental response (dark solid), CREATE-L (light), RCDM (dashed). The CREATE-L and RCDM responses cannot be distinguished because they are very similar.

FIG. 12. Comparison of the experimental, CREATE-L and RCDM responses of zIp to antisymmetric RBS stimulation. Experimental response (dark solid), CREATE-L (light), RCDM (dashed).

FIG. 13. Comparison of the experimental, CREATE-L and plasmaless CREATE-L responses to symmetric square pulse stimulation on the E coils. Experimental response (dark solid), CREATE-L (light), plasmaless CREATE-L (dashed).

FIG. 14. Comparison of the experimental, CREATE-L and plasmaless CREATE-L responses to symmetric square pulse stimulation on the F coils. Experimental response (dark solid), CREATE-L (light), plasmaless CREATE-L (dashed).

FIG. 15. Comparison of the experimental, CREATE-L and plasmaless CREATE-L responses to symmetric square pulse stimulation on the OH coils. Experimental response (dark solid), CREATE-L (light), plasmaless CREATE-L (dashed).

FIG. 16. Comparison of the experimental, CREATE-L and plasmaless CREATE-L responses of P_VERT to symmetric RBS stimulation. Experimental response (dark solid), CREATE-L (light), plasmaless CREATE-L (dashed).

FIG. 17. Comparison of the experimental, CREATE-L and plasmaless CREATE-L responses of TRI_OUT to symmetric RBS stimulation. Experimental response (dark solid), CREATE-L (light), plasmaless CREATE-L (dashed).

FIG. 18. Comparison of the experimental, CREATE-L and plasmaless CREATE-L responses of TRI_IN to symmetric RBS stimulation. Experimental response (dark solid), CREATE-L (light), plasmaless CREATE-L (dashed).

FIG. 19. Comparison of the experimental, CREATE-L and plasmaless CREATE-L responses of Ip to symmetric RBS stimulation. Experimental response (dark solid), CREATE-L (light), plasmaless CREATE-L (dashed).

FIG. 20. Comparison of the experimental, CREATE-L and plasmaless CREATE-L responses of Ψ_R to symmetric RBS stimulation. Experimental response (dark solid), CREATE-L (light), plasmaless CREATE-L (dashed).

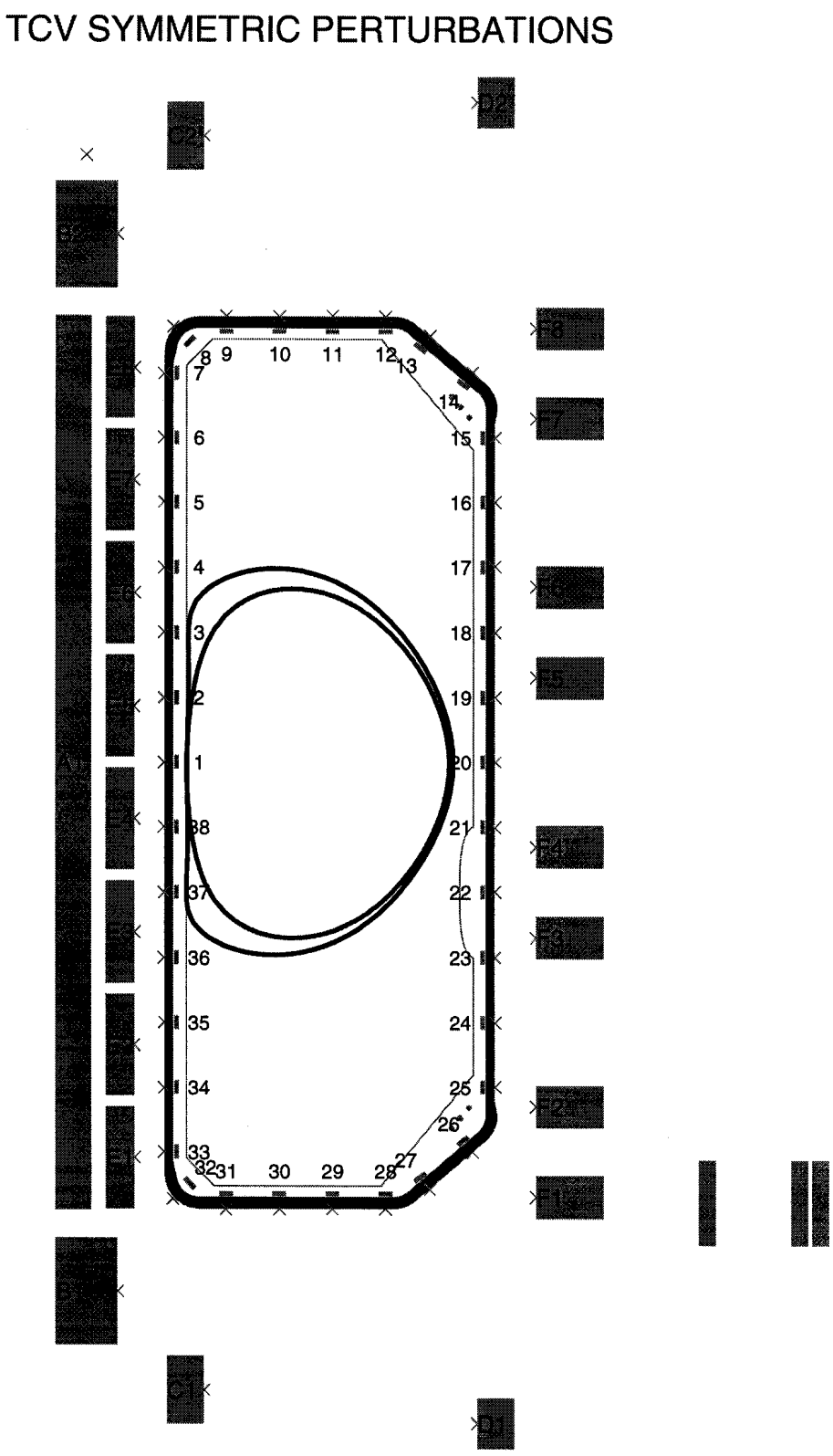

FIG. 1. The TCV vacuum vessel, poloidal field coils, poloidal field probes (marked '-' inside the tiles) and flux loops (marked 'x'). The last closed flux surface contours shown (#10857) correspond to limits of variation during up-down symmetric excitation of the E-coils: B_ϕ=1.4T, I_p≈200kA, q_a≈5.

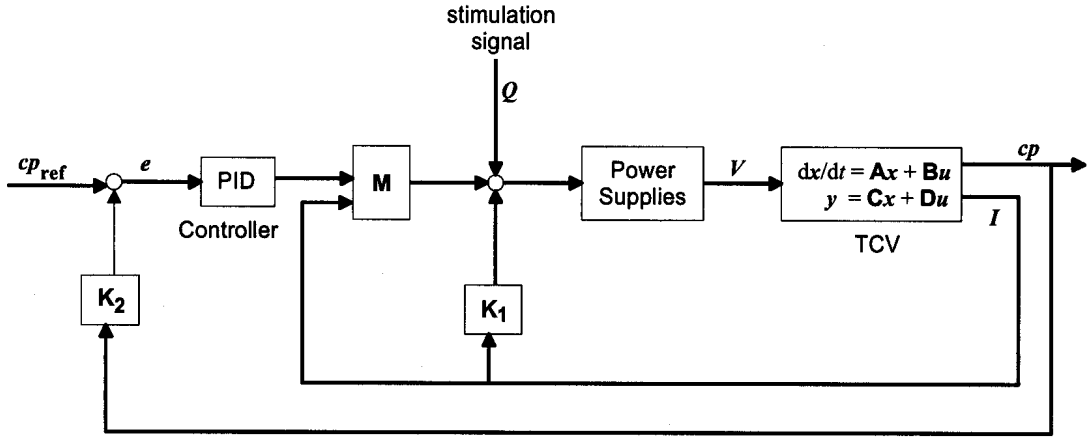

FIG. 2. Schematic diagram of the TCV control system.

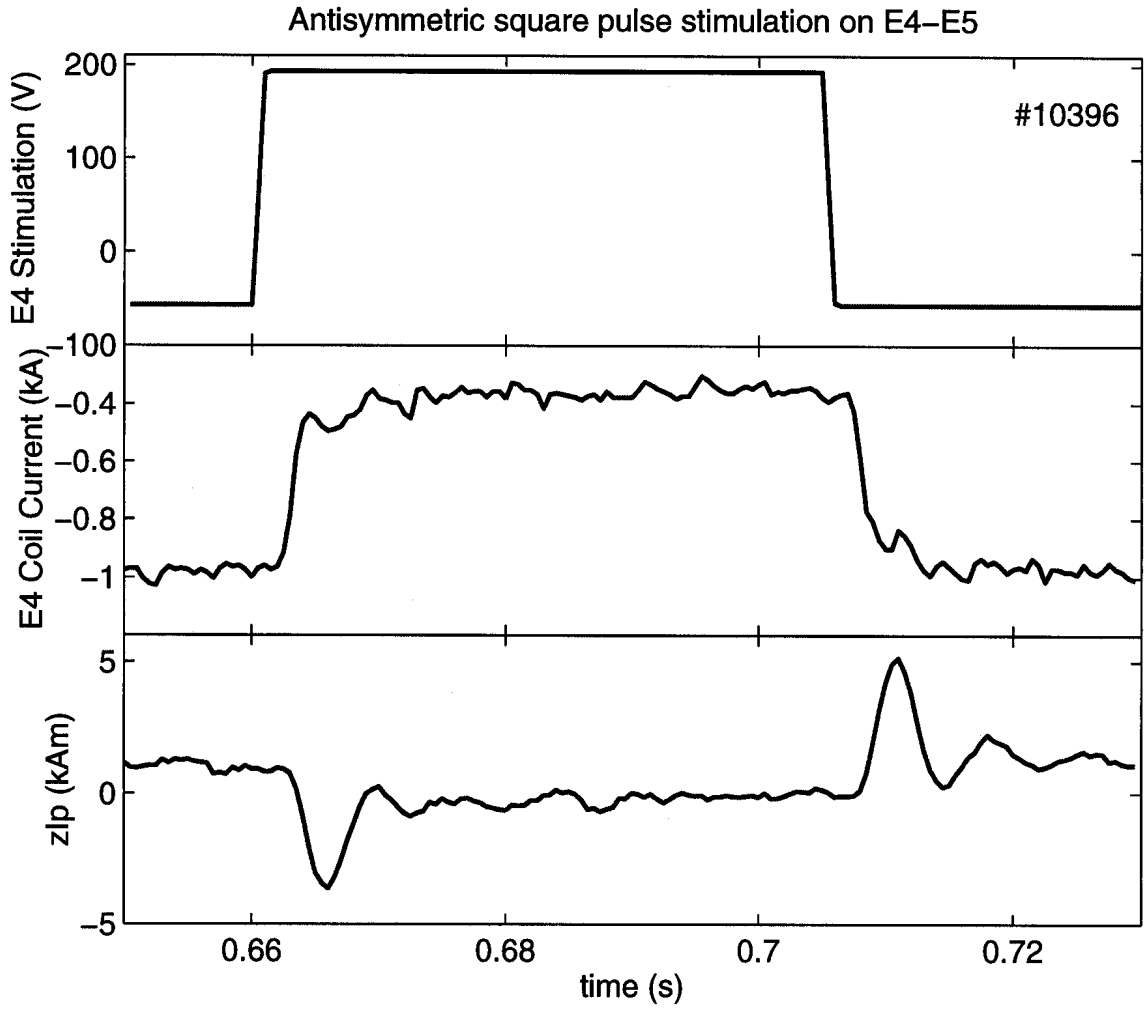

FIG. 3. Effect of square pulse stimulation applied to the E4-E5 coil pair.

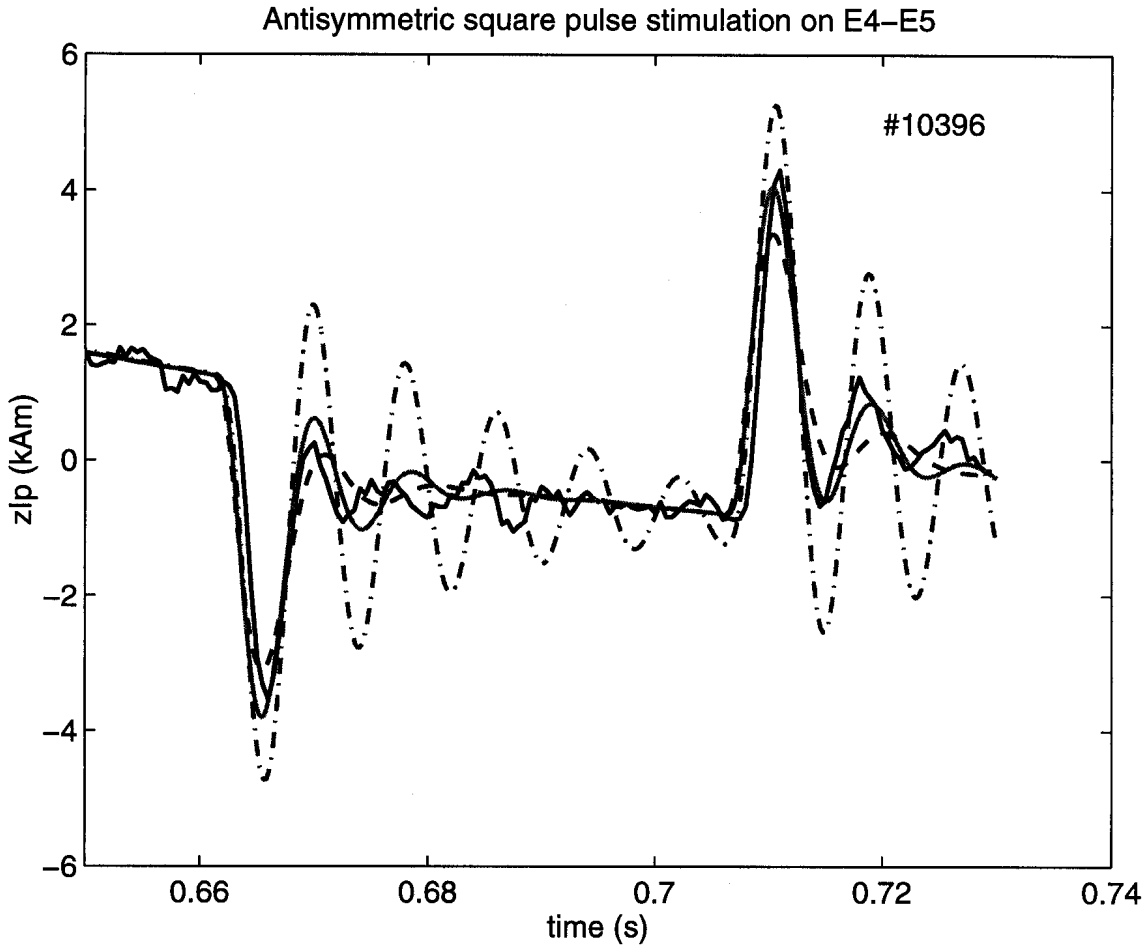

FIG. 4. Comparison of the experimental response to simulated responses using CREATE-L models with different power supply poles. Square pulse stimulation was applied to coil pair E4-E5. Experimental response (dark solid), model with no power supply pole (dashed), model with pole at 1/0.3ms (light solid), and model with pole at 1/0.6ms (dash dotted).

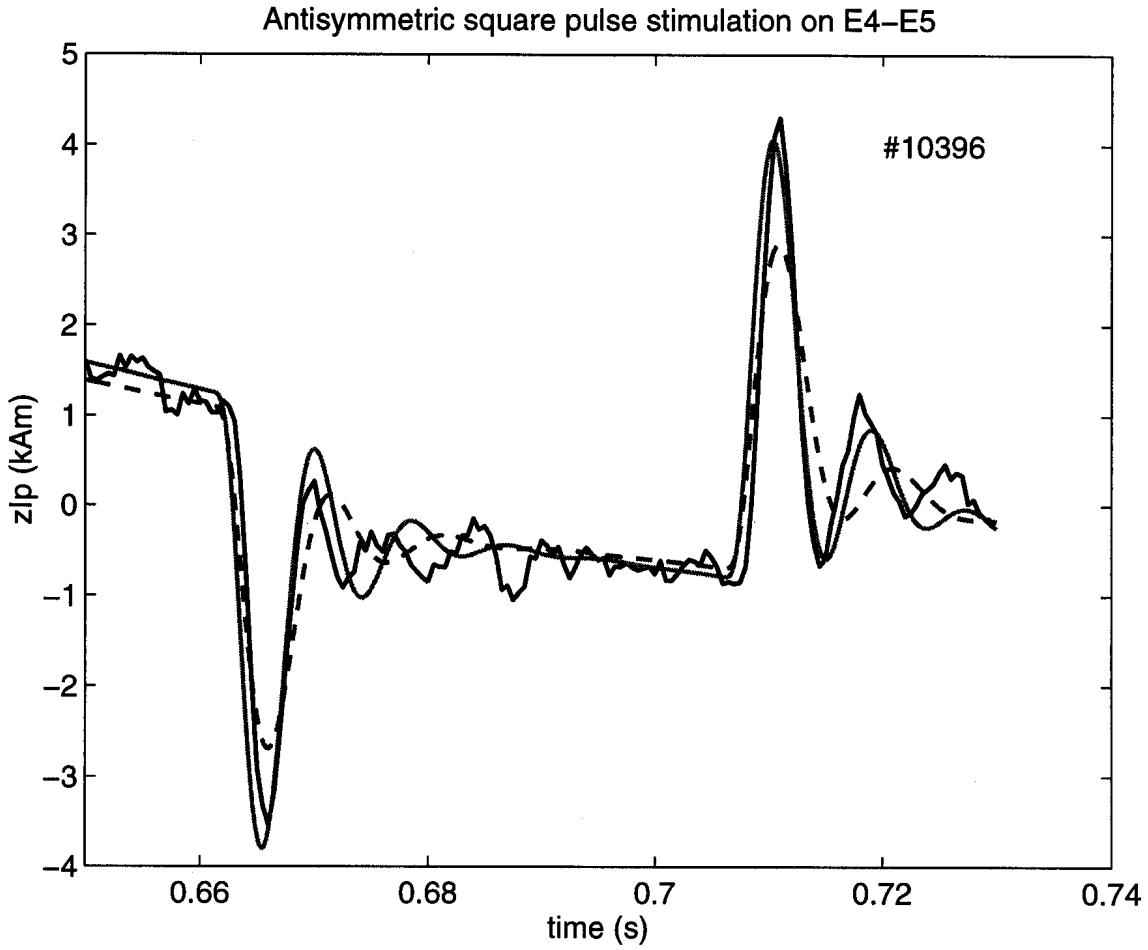

FIG. 5. Comparison of the experimental response to CREATE-L and RCDM models for square pulse stimulation applied to the E4-E5 coil pair. Experimental response (dark solid), CREATE-L model (light solid), and RCDM model (dashed).

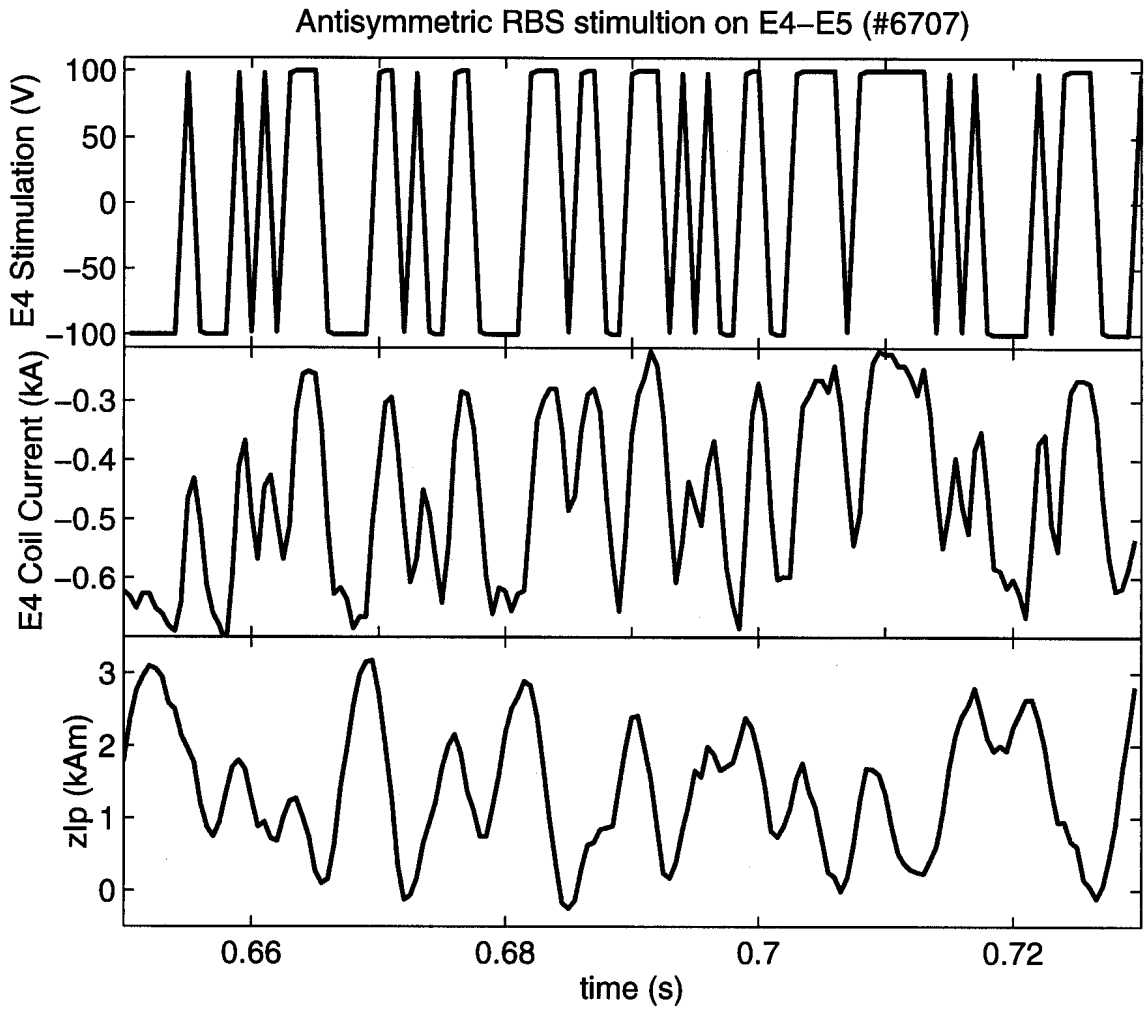

FIG. 6. Effect of RBS stimulation applied to the E4-E5 coil pair.

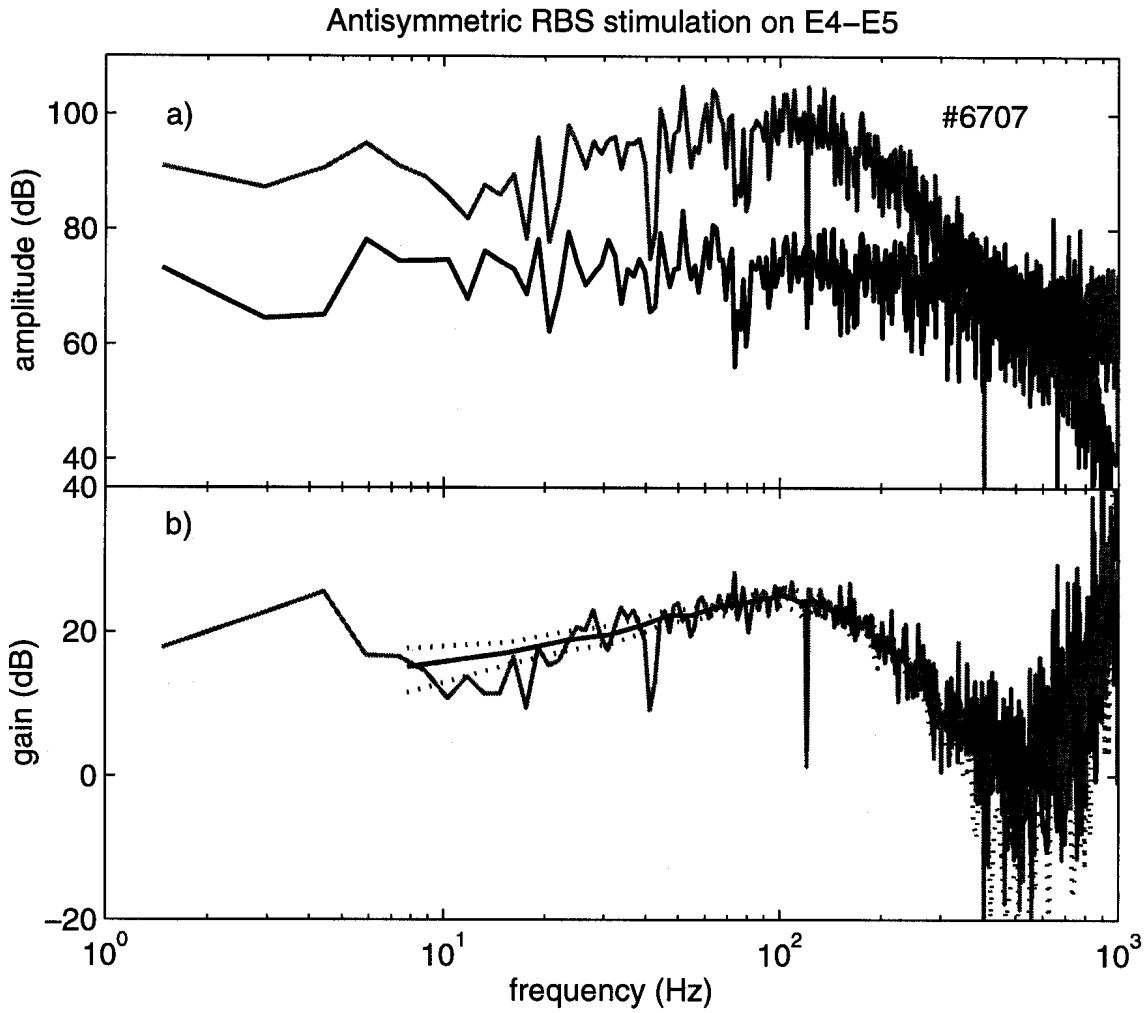

FIG. 7. a) Discrete Fourier Transform of RBS stimulation signal on the E4-E5 coil pair (dark) and zIp response (light). b) Estimates of closed loop transfer function using ETFE method and spectral analysis. ETFE estimate (light solid), and spectral analysis estimate (dark solid) with associated +/- 3 standard deviation bounds (dotted)

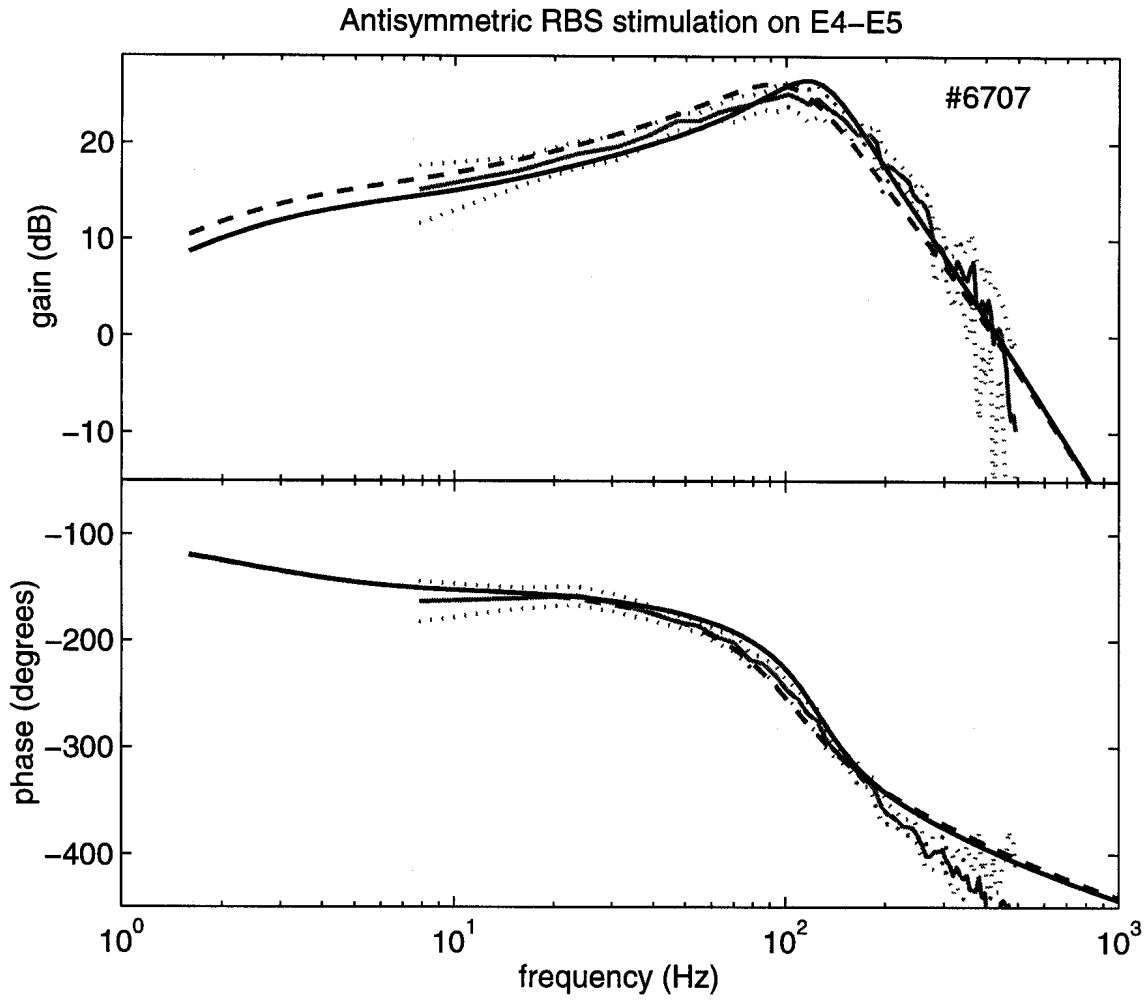

FIG. 8. Bode plot comparison of experimental against CREATE-L and RCDM closed loop transfer function from stimulation on the E4-E5 coil pair to zIp. Experimental spectral analysis estimate (light solid) with associated +/- 3 standard deviation bounds (dotted), CREATE-L model (dark solid) and RCDM model (dotted).

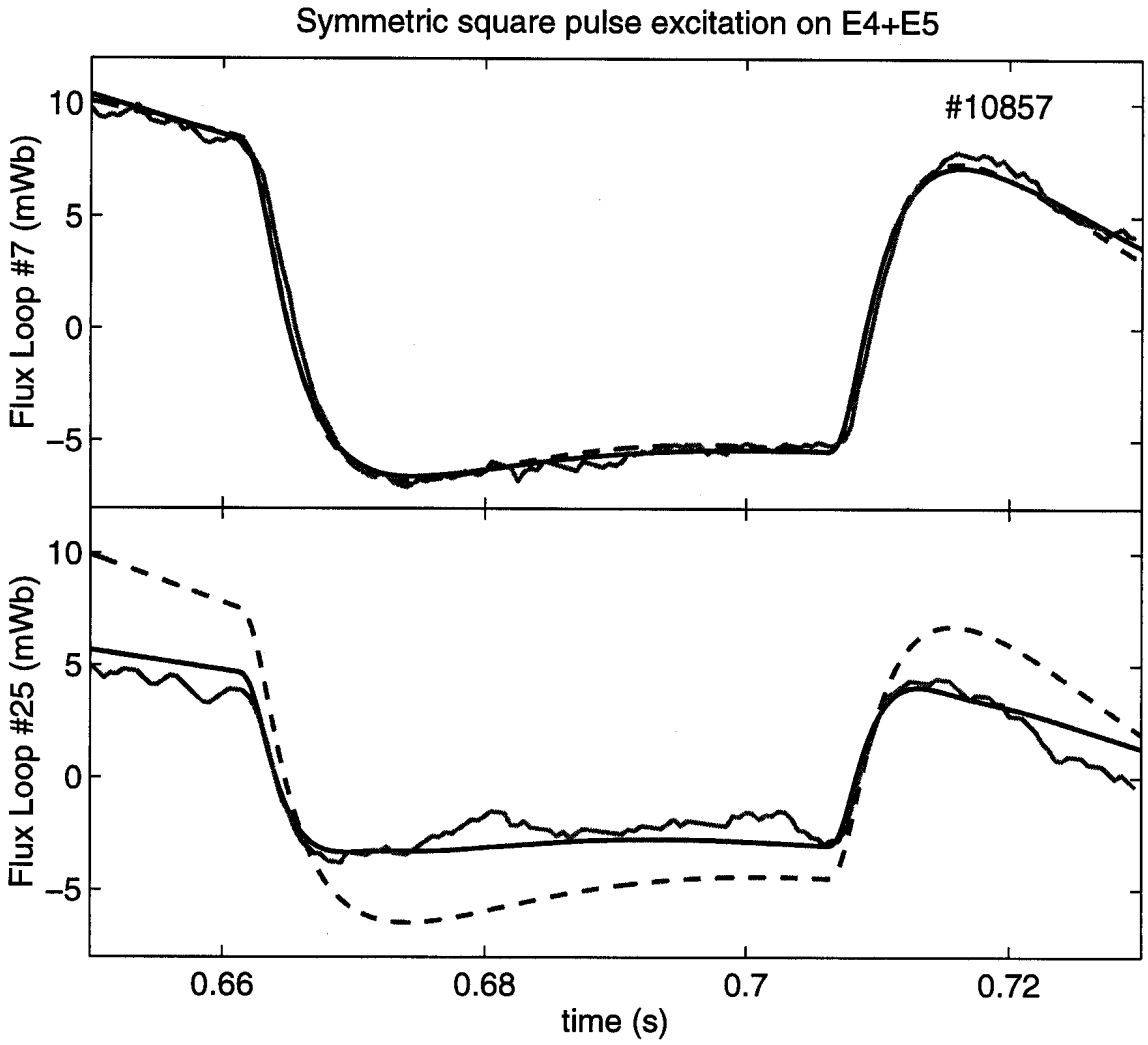

FIG. 9. Comparison of experimental and modelled responses of flux as measured by two different flux loops to square pulse stimulation on the E4+E5 coil pair. Experimental measurement (light solid), CREATE-L model (dark solid) and plasmaless CREATE-L model (dotted).

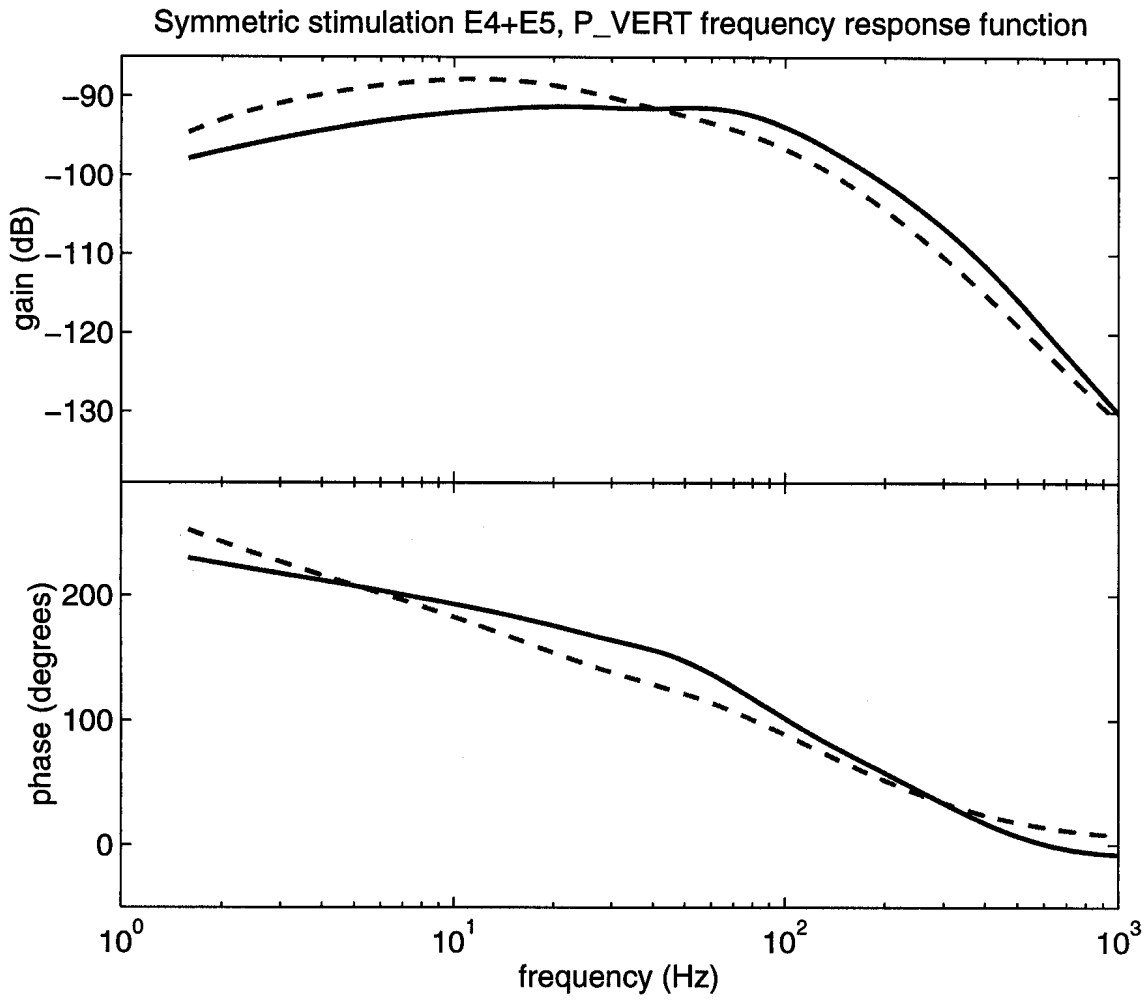

FIG. 10. Comparison of frequency response functions for the P_VERT control parameter for stimulations using the coil pair E4+E5. CREATE-L model (solid) and plasmaless CREATE-L model (dotted).

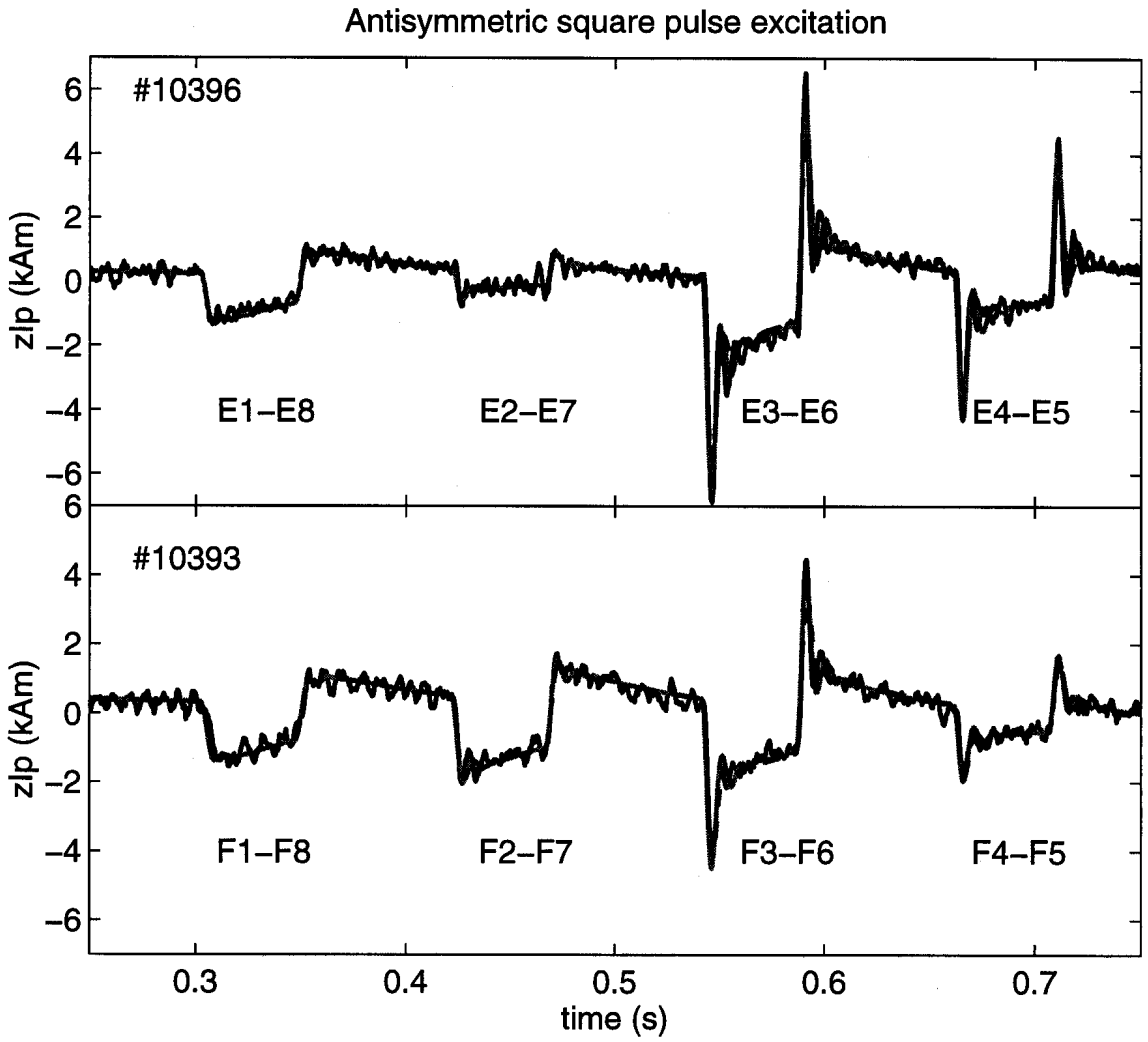

FIG. 11. Comparison of the experimental, CREATE-L and RCDM responses to antisymmetric square pulse stimulation on the E and F coils. Experimental response (dark solid), CREATE-L (light), RCDM (dashed). The CREATE-L and RCDM responses cannot be distinguished because they are very similar.

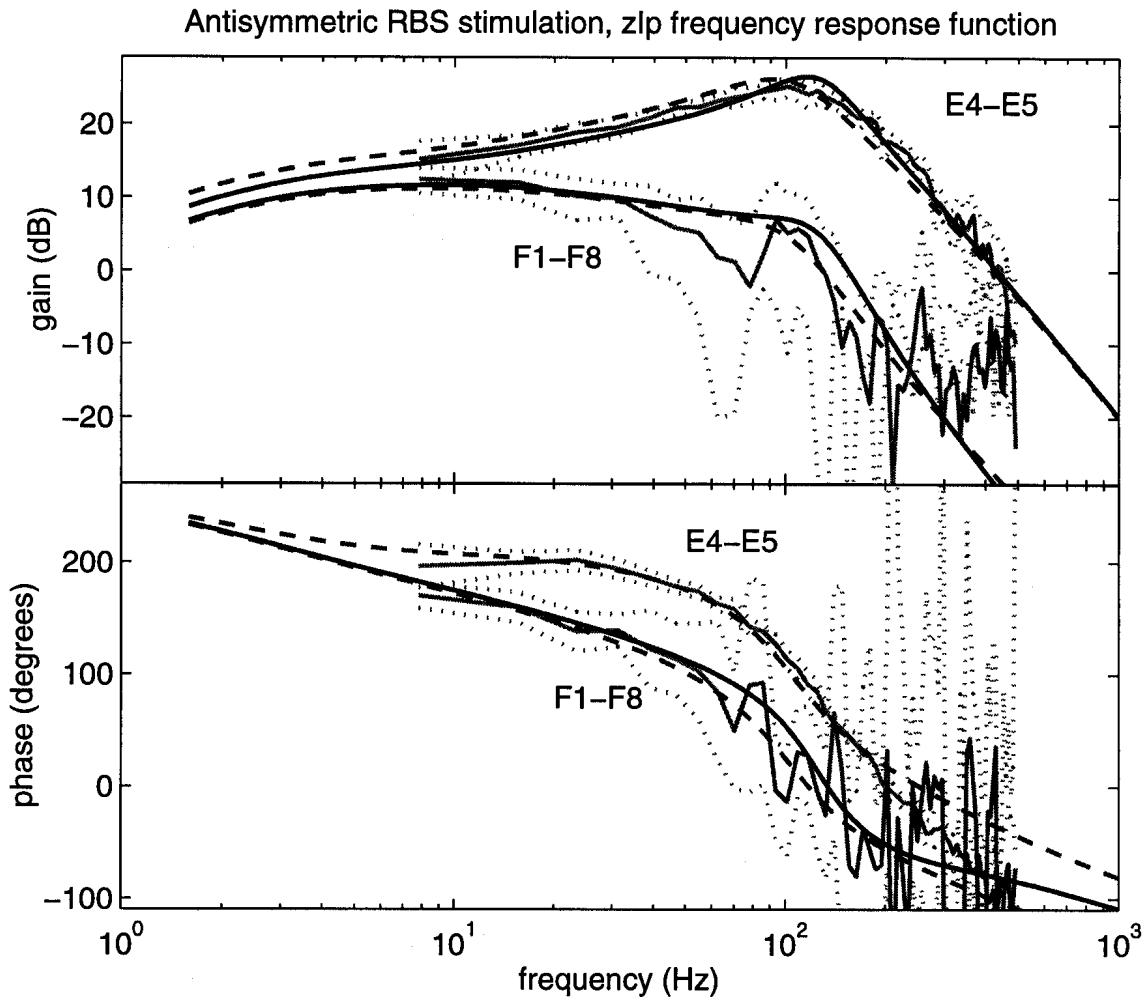

FIG. 12. Comparison of the experimental, CREATE-L and RCDM responses of zIp to antisymmetric RBS stimulation. Experimental response (dark solid), CREATE-L (light), RCDM (dashed).

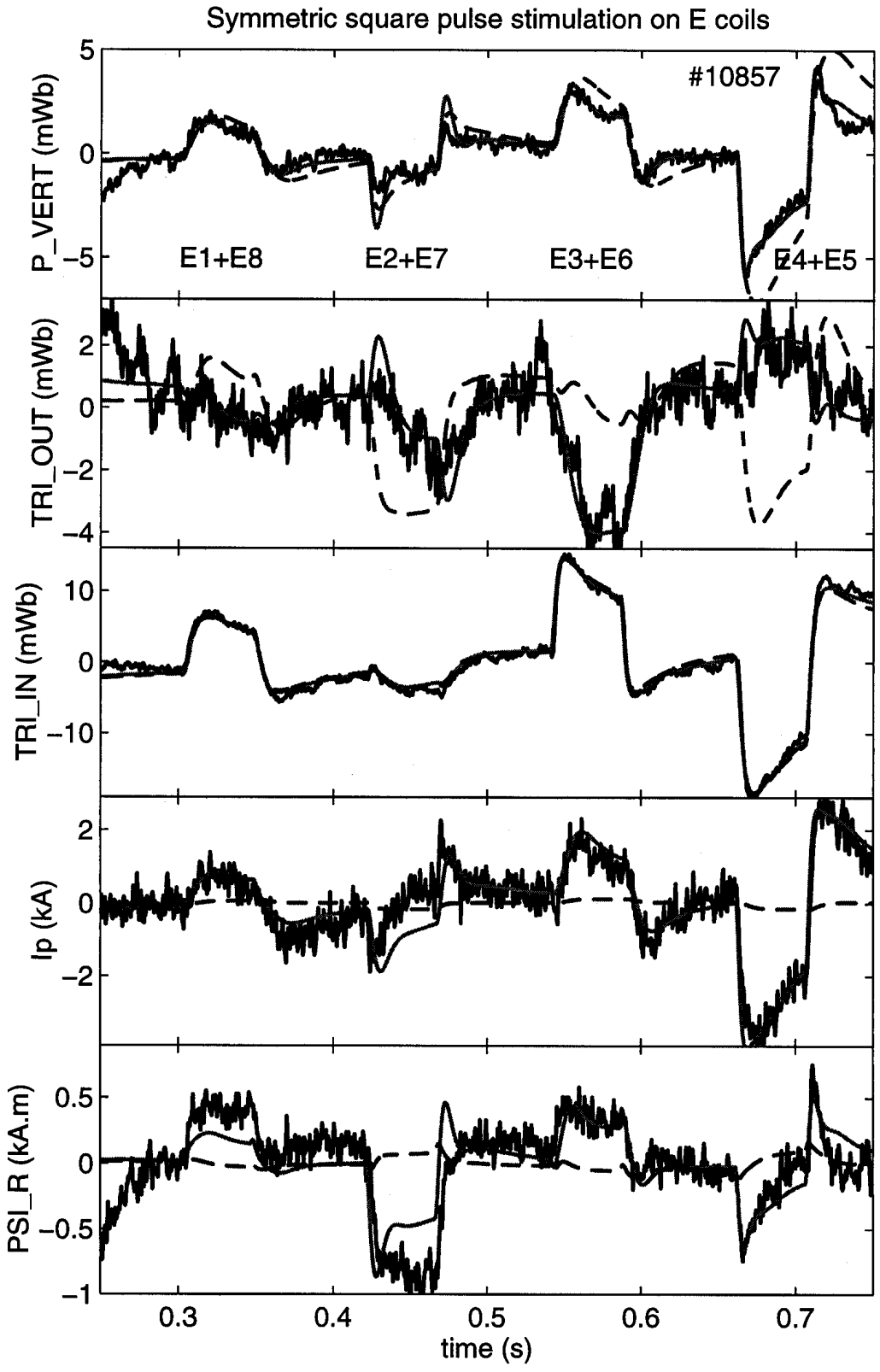

FIG. 13. Comparison of the experimental, CREATE-L and plasmaless CREATE-L responses to symmetric square pulse stimulation on the E coils. Experimental response (dark solid), CREATE-L (light), plasmaless CREATE-L (dashed).

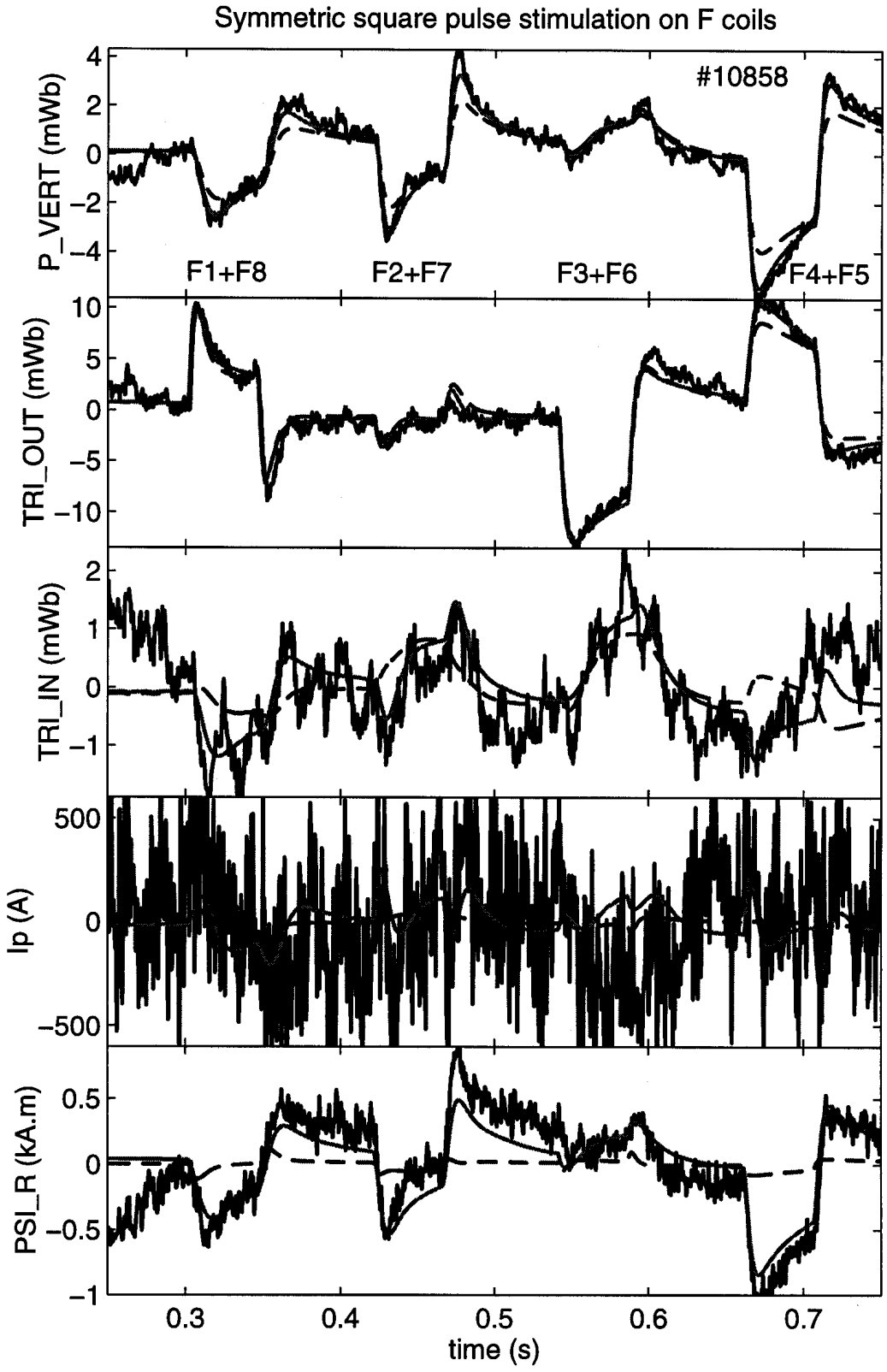

FIG. 14. Comparison of the experimental, CREATE-L and plasmaless CREATE-L responses to symmetric square pulse stimulation on the F coils. Experimental response (dark solid), CREATE-L (light), plasmaless CREATE-L (dashed).

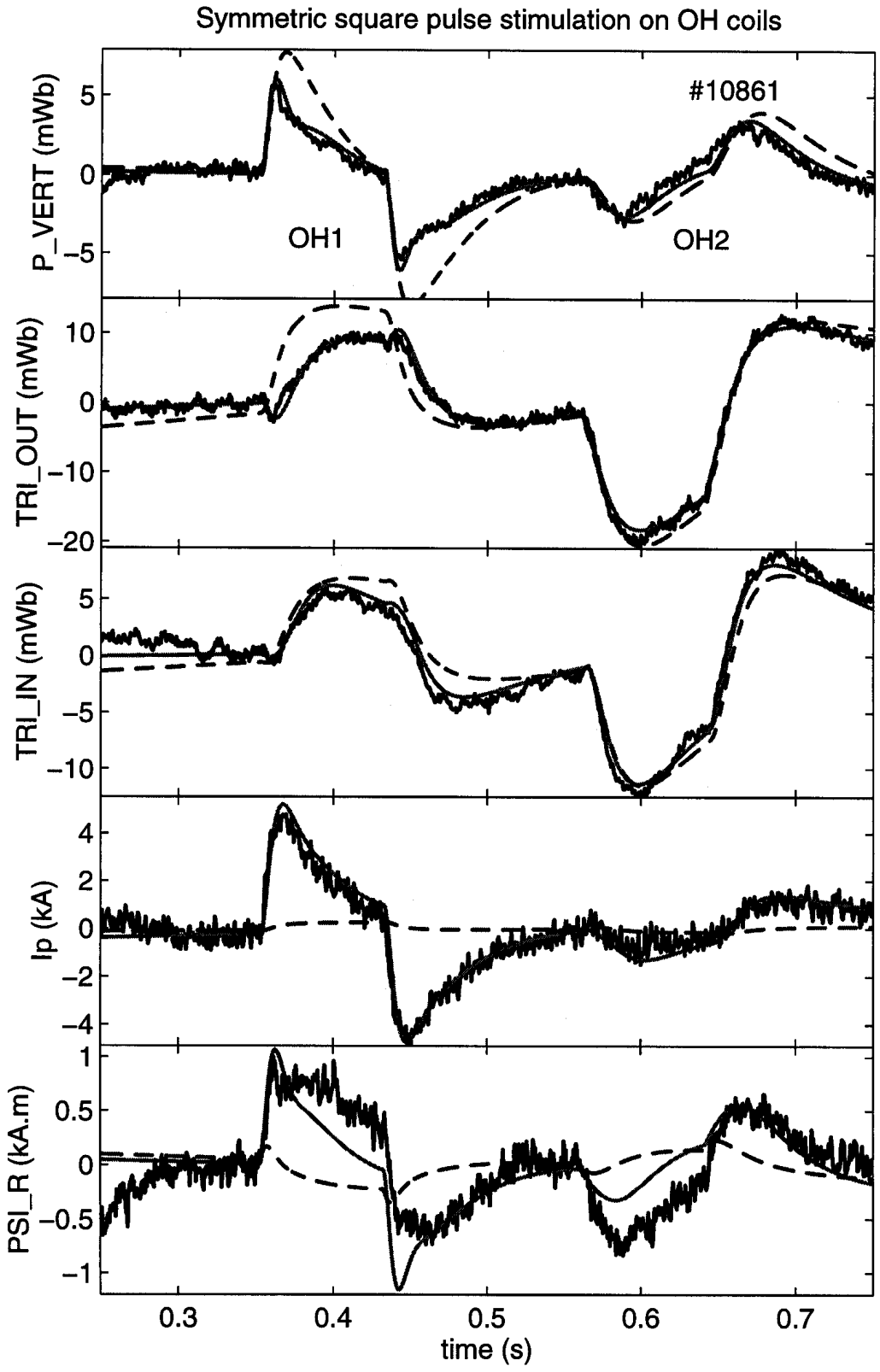

FIG. 15. Comparison of the experimental, CREATE-L and plasmaless CREATE-L responses to symmetric square pulse stimulation on the OH coils. Experimental response (dark solid), CREATE-L (light), plasmaless CREATE-L (dashed).

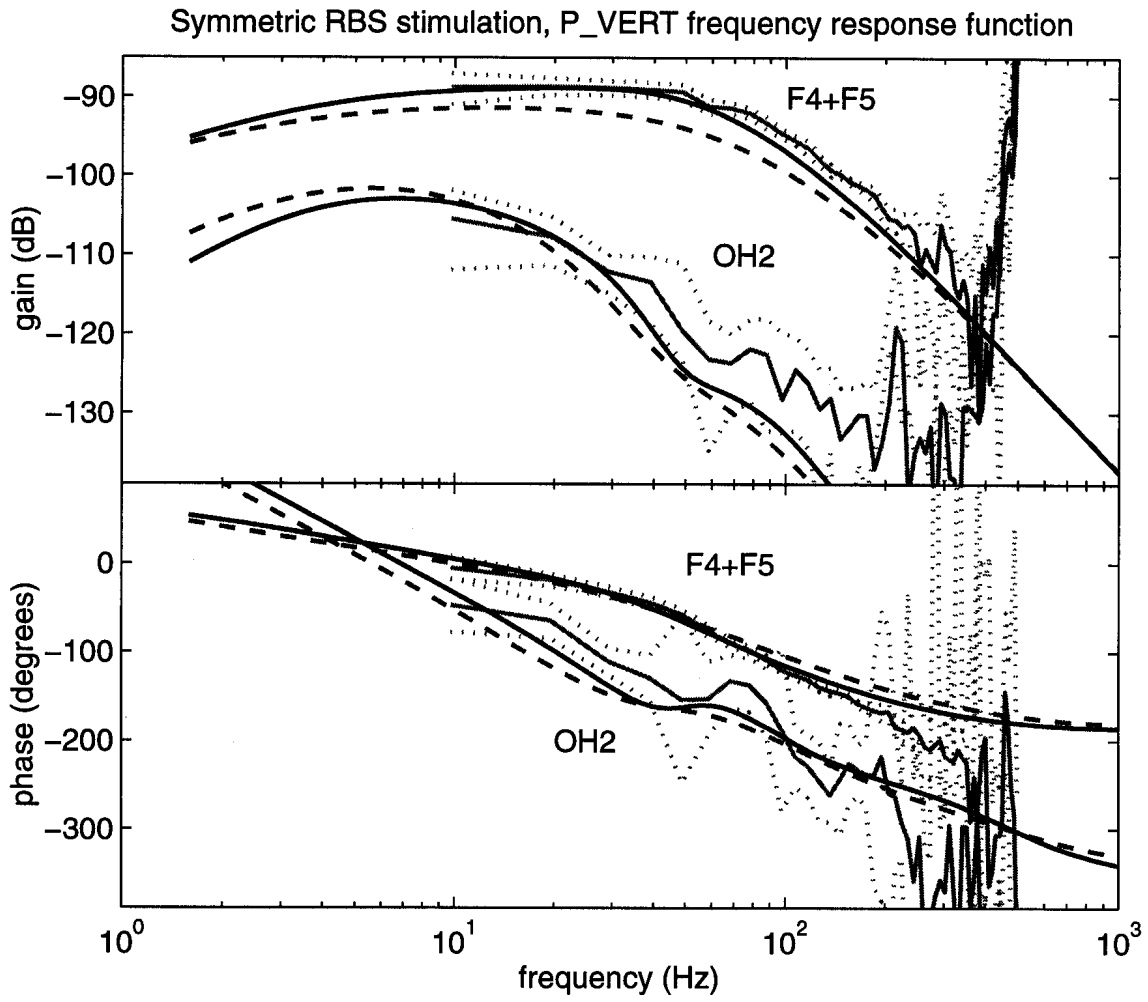

FIG. 16. Comparison of the experimental, CREATE-L and plasmaless CREATE-L responses of P_VERT to symmetric RBS stimulation. Experimental response (dark solid), CREATE-L (light), plasmaless CREATE-L (dashed).

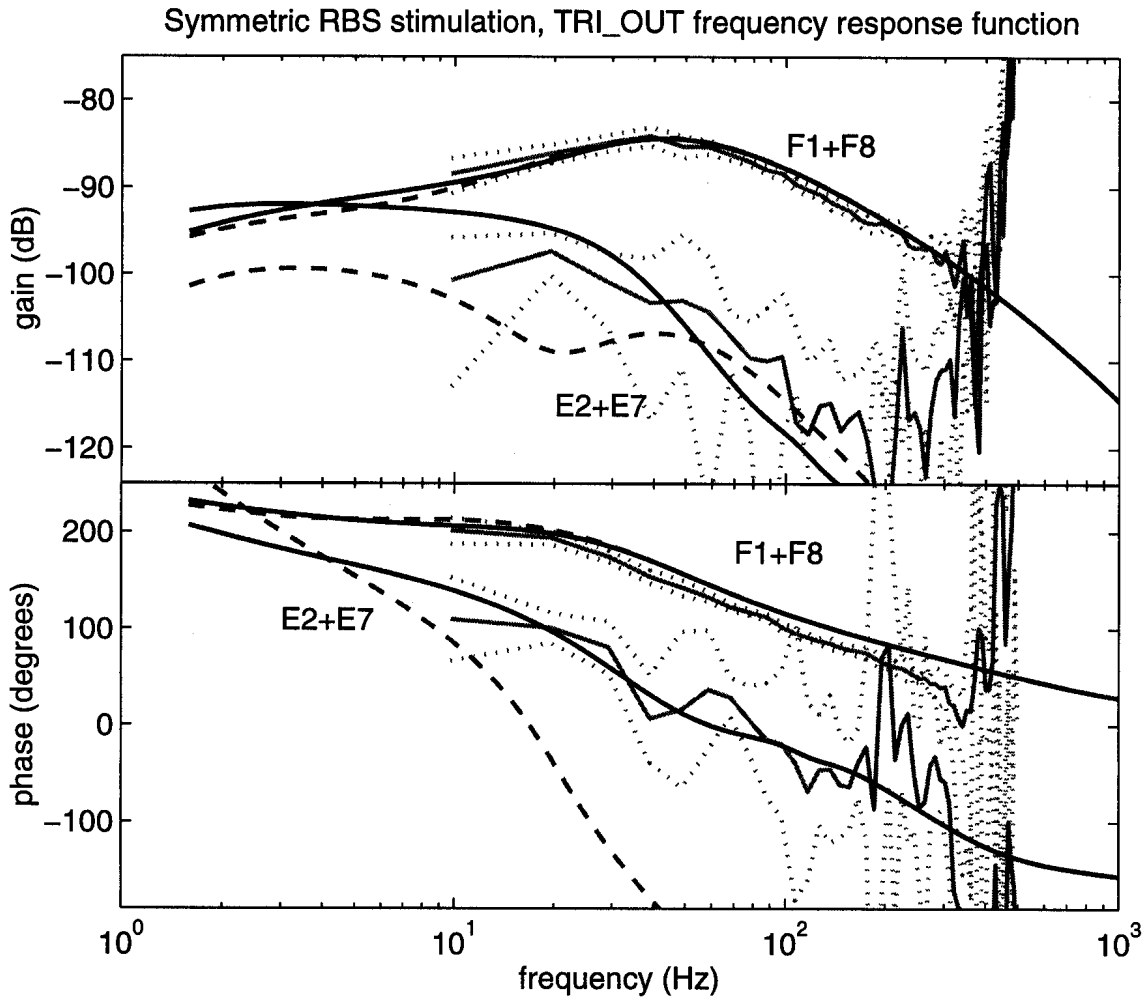

FIG. 17. Comparison of the experimental, CREATE-L and plasmaless CREATE-L responses of TRI_OUT to symmetric RBS stimulation. Experimental response (dark solid), CREATE-L (light), plasmaless CREATE-L (dashed).

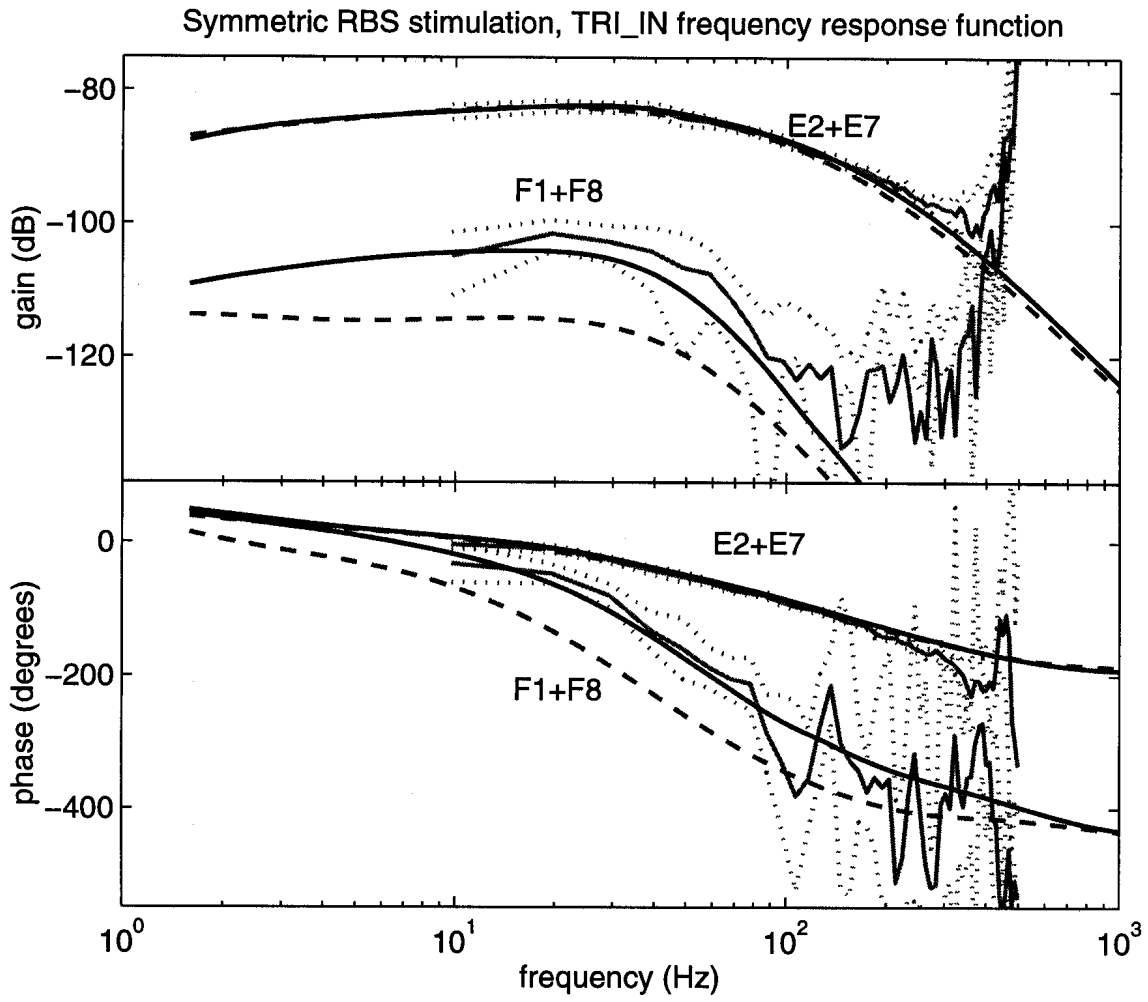

FIG. 18. Comparison of the experimental, CREATE-L and plasmaless CREATE-L responses of TRI_IN to symmetric RBS stimulation. Experimental response (dark solid), CREATE-L (light), plasmaless CREATE-L (dashed).

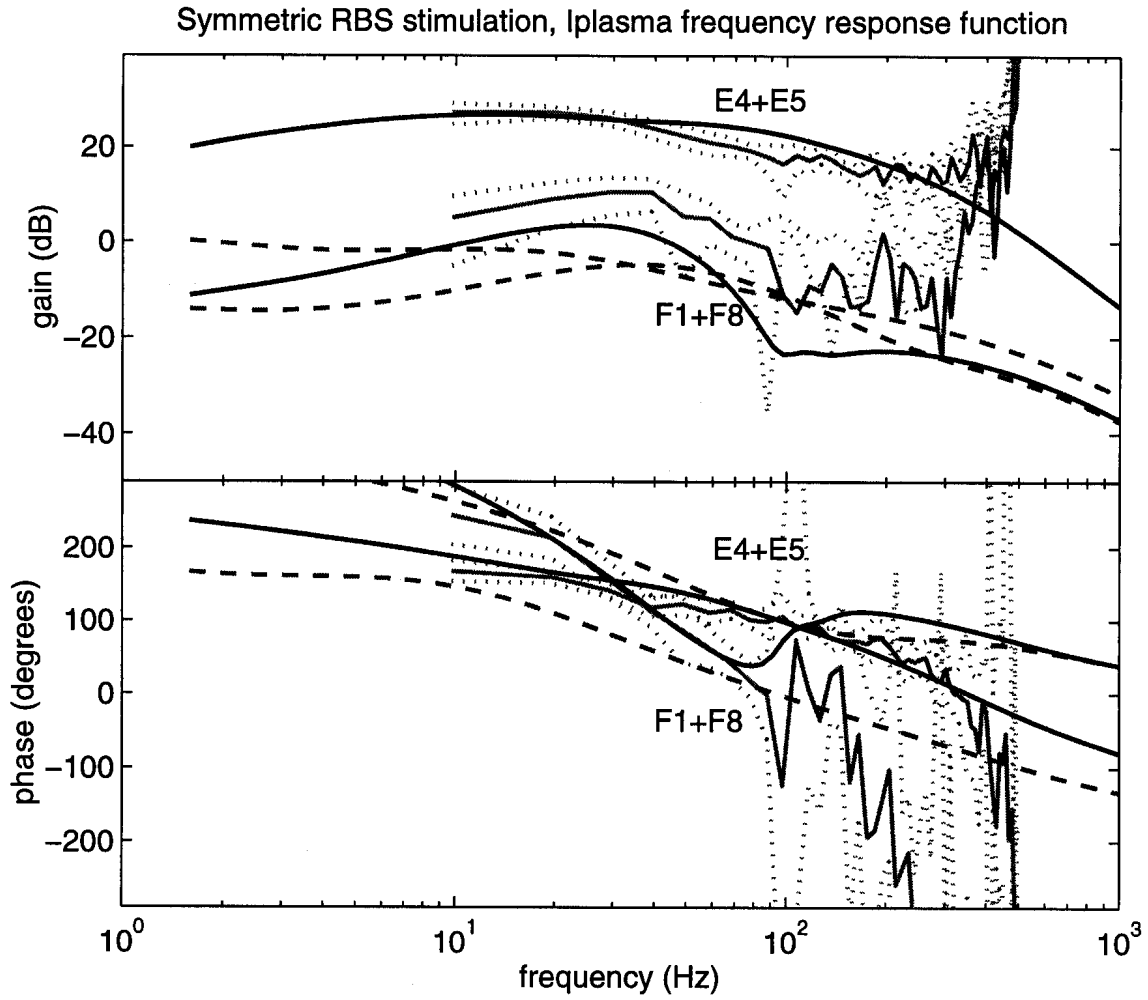

FIG. 19. Comparison of the experimental, CREATE-L and plasmaless CREATE-L responses of Ip to symmetric RBS stimulation. Experimental response (dark solid), CREATE-L (light), plasmaless CREATE-L (dashed).

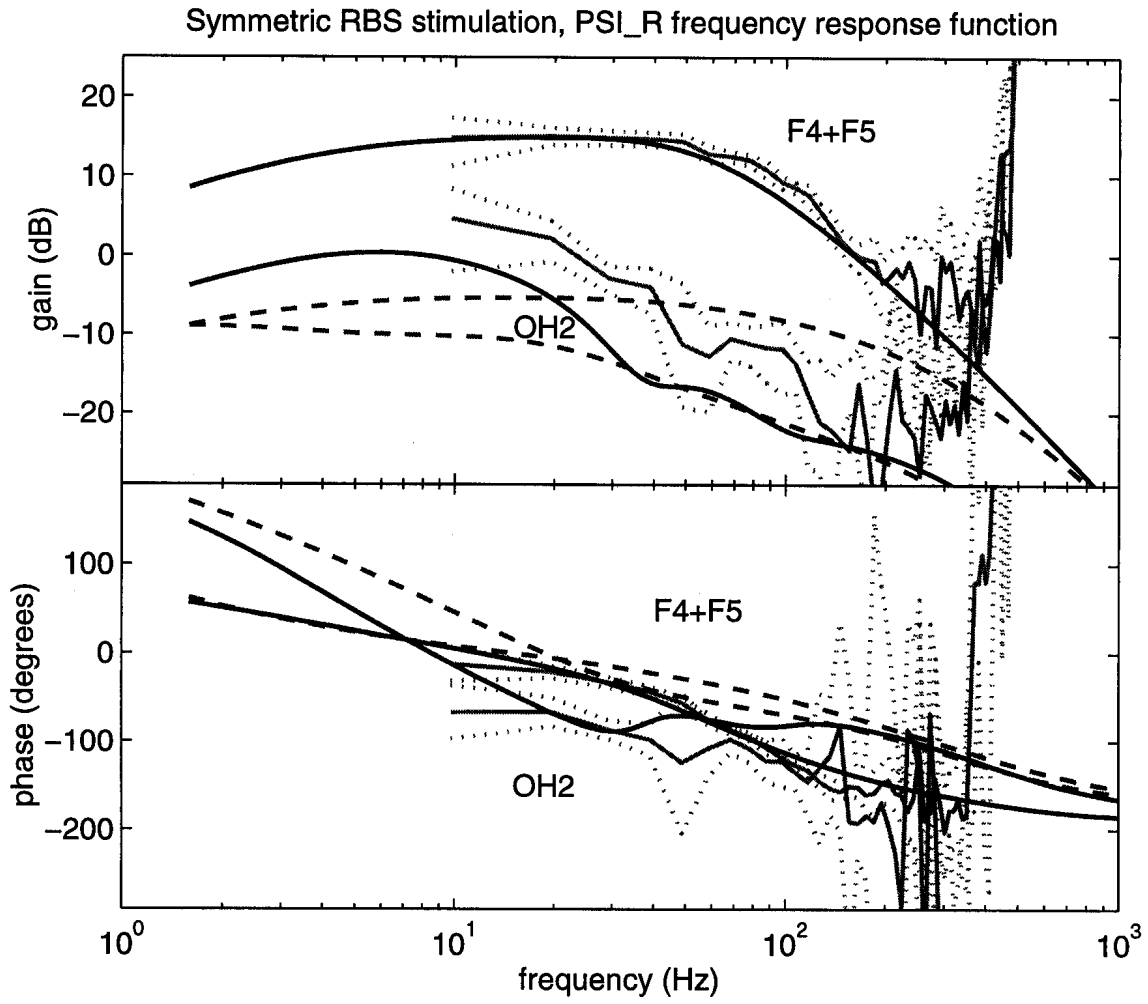

FIG. 20. Comparison of the experimental, CREATE-L and plasmaless CREATE-L responses of Ψ_R to symmetric RBS stimulation. Experimental response (dark solid), CREATE-L (light), plasmaless CREATE-L (dashed).